The Health Assessment of Lithium-ion Batteries Using Machine Learning

by

Lucas Murphy
BASc., Queen's University, 2020

A Dissertation Submitted in Partial Fulfillment of the
Requirements for the Degree of

MASTER OF APPLIED SCIENCE

in the Department of Mechanical Engineering

The Rapid Health Assessment of Lithium-ion Batteries Using Machine Learning

by

Lucas Murphy
BASc., Queen's University, 2020

Supervisory Committee

Dr. Curran Crawford, Supervisor
(Department of Mechanical Engineering)

Dr. Zoumin Dong, Committee Member
(Department of Mechanical Engineering)

ABSTRACT

Lithium-ion batteries are emerging as a crucial technology in the world's clean energy transition. These batteries face challenges as they degrade with use due to unwanted chemical side reactions. In this thesis, we propose two methods of using relatively accessible battery data to predict important health metrics. These health metrics improve battery safety, control, and decision-making.

In the first method, we leverage battery charging times to decipher measures of internal chemical degradation. Using machine learning, different modes of degradation can be attributed to segments of the constant current and constant voltage charging curves. This model is trained and tested using cells cycled under varying depths of discharge and C-rate conditions inducing an array of degradation pathways. We can gather insights into the model's learning through input feature analysis to determine key areas within the charging regime.

At the end of the battery's first life, we can analyze its degradation modes to determine its viability in second-life applications. This is conducted by using features extracted from electrochemical impedance spectroscopy as input data to a binary classifier. This determines whether a battery should be reused or recycled. The distinction is made based on a metric that includes the current state of health of the battery, and the slope of capacity degradation to the end of second life.

These contributions look to quantify variance and non-linearity in Lithium-ion battery degradation to inform economic and safety-based decision-making. These contributions also address challenges in data-driven battery modelling regarding model explainability and data scarcity.

Contents

List of Tables

List of Figures

List of Abbreviations

General Concepts	
LIB	Lithium-ion Battery
EV	Electric Vehicle
ESS	Energy Storage System
SLB	Second Life Battery
Battery Modeling and Machine Learning	
ECM	Equivalent Circuit Model
ML	Machine Learning
VAE	Variational Autoencoder
SOH	State of Health
SOC	State of Charge
RUL	Remaining Useful Life
EOL	End of Life
Battery Testing and Diagnostics	
BMS	Battery Management System
EIS	Electrochemical Impedance Spectroscopy
OCV	Open Circuit Voltage
DOD	Depth of Discharge
CC	Constant Current
CV	Constant Voltage
CCCT	Constant Current Charging Time
CVCT	Constant Voltage Charging Time
TCT	Total Charging Time
Battery Degradation	
DM	Degradation Mode
CL	Conductivity Loss
LLI	Loss of Lithium Inventory
LAM	Loss of Active Material
SEI	Solid Electrolyte Interphase
CT	Charge Transfer

ACKNOWLEDGEMENTS

I would like to thank:

My girlfriend Kenzie for being my biggest supporter and always lifting me up when I am down. I hope I can do the same for you as you finish your PhD.

My Family for always offering unsolicited academic advice, encouragement, and continuous support.

Dr. Curran Crawford for introducing me to the world of energy systems and making my Master's a very positive experience. I would also like to thank Curran for his financial support and unwavering patience over the past few years.

My friends in Victoria who have helped make my time here the best years of my life so far.

My friends in SSDL and IESVIC, thank you for the stimulating discussions around energy systems, I learned so much from all of you.

Jules Pare and Sean Buchanan for their work in the PRIMED battery lab curating data used in this thesis.

Pulsenics and Rainhouse for providing valuable industry knowledge and equipment that made this research possible.

Chapter 1

Introduction

As global temperatures rise, nations are pledging to lower carbon emissions to net zero levels by 2050 following the Paris Agreement. Proposed Canadian climate policies to aid in reaching this goal include zero-emission vehicle sales targets reaching 100% by 2035 for new light-duty vehicles [5]. This accounts for approximately 15% of Canada's carbon emissions [6, 7]. Policies of this kind will see an exponential increase in Lithium-ion battery (LIB) production, followed by an equivalent rise in battery retirement. The LIB retirement boom is slated to occur over the next ten years. This will result in a call for innovation in the battery recycling and reuse industries [1].

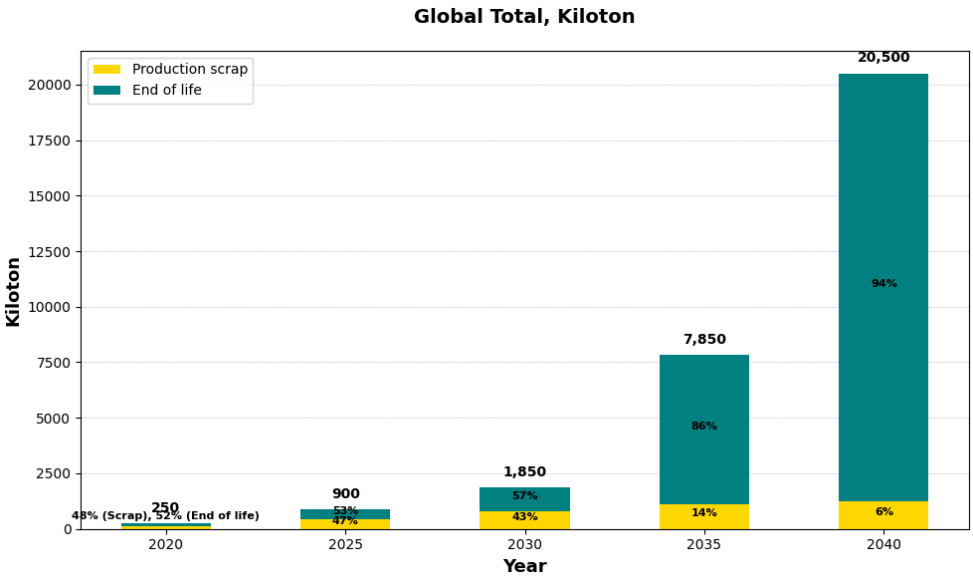

Figure 1.1: Projection of retired lithium-ion batteries between the years 2020 and 2040. Adapted from Mckinsey [1]

Electric vehicle (EV) batteries are typically retired once they reach 60-80% of their initial capacity, also known as the state of health (SOH). This affects the battery range leading owners to retire the vehicle after an average of 10-12 years [8]. Battery recycling and reuse can be used to create a closed-loop system to reduce the initial emissions associated with extracting minerals and battery manufacturing. Based on life cycle analysis, EVs reduce greenhouse gas emissions anywhere between 20 and 70%, depending on the country's electricity generation and vehicle operation [9]. This will rise rapidly with the adoption of clean electricity generation, in turn increasing the requirement for energy storage systems (ESS). When used as an ESS for stationary, residential PV, utility PV, or EV fast charging applications, second-life batteries reduce greenhouse gas emissions between 10 and 80% compared to new LIBs [10, 11, 12]. Figure 1.2 provides a lifetime trajectory of Lithium-ion batteries in relation to the battery capacity, and life cycle milestones [13, 14]. This figure highlights the volatility in second-life aging as batteries experience rapid capacity fade of varying degrees at some point during their lifetime[15].

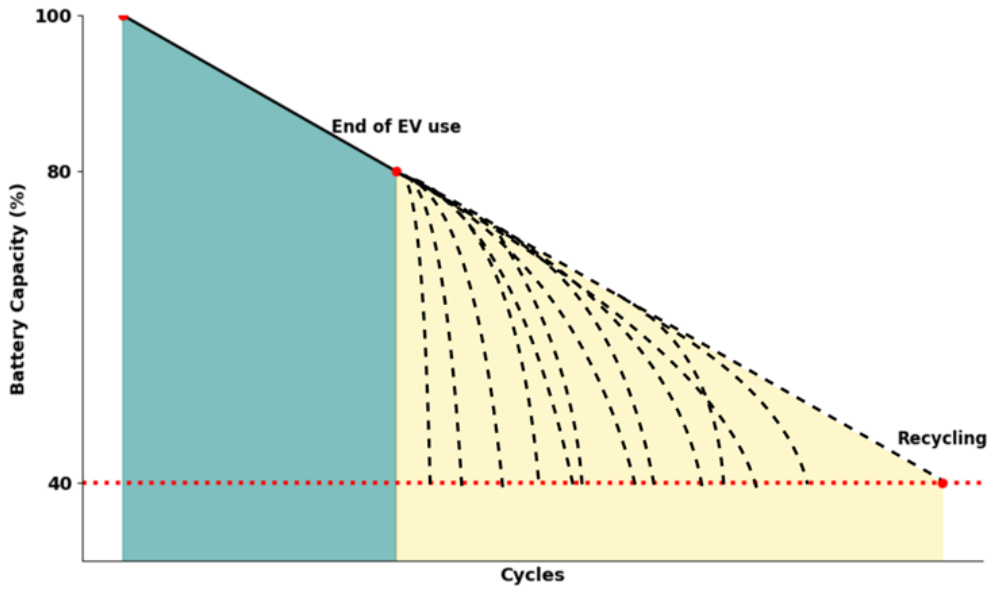

Figure 1.2: A simplified battery capacity trajectory segmented into first and second life.

1.1 Lithium-ion battery degradation

LIBs age due to complex internal chemical and physical degradation. To facilitate the integration and success of LIBs, operational, economic, safety, and lifespan factors must be considered. Operating conditions such as depth of discharge, discharge/charge rate, and temperature significantly affect battery capacity and power by inciting degradation mechanisms [16]. Chemical and physical degradation mechanisms increase battery internal resistance, which affects battery performance and can lead to thermal runaway. Degradation mechanisms such as electrode cracking, lithium-plating, and electrolyte decomposition can be categorized by their influence on the battery [17, 18]. These categories are denoted as degradation modes, which include the loss of conductivity, lithium inventory, and active material. With varying operating conditions between systems, this degradation can be unpredictable, raising a need for methods of monitoring and forecasting battery performance [15].

We conduct cycle testing under various operating conditions and record data to better understand battery stressors and their influence on degradation. While tracking current, voltage, capacity, and temperature data, characterization tests are used to reveal information regarding the batterys health. This includes slow-charging cycles and rapid current perturbations using tests such as high-powered pulse characterization, impedance spectroscopy, and incremental capacity analysis to discern degradation modes [19]. This data is used to develop models that provide key insights such as battery SOH, state of charge (SOC), and remaining useful life (RUL). These metrics help inform decision-making regarding safety, control, and retirement planning.

When executing battery characterization tests in the field, the resources, data analysis difficulty, and time required to complete testing dictate the feasibility of implementation. Electrochemical impedance spectroscopy (EIS) is a useful method of battery characterization as it takes less than 5 minutes and can be performed during battery operation with recent technology developments. EIS operates by sending an AC signal at various frequencies and computing impedance based on the resulting voltage response. This impedance provides insights into the batterys internal degradation of different paced processes based on the applied frequency, such as voltage drop, charge transfer, and diffusion [20, 21].

1.2 Lithium-ion battery modelling

LIB modelling is commonly categorized into electrochemical, black-box, and grey-box techniques. Electrochemical models such as the pseudo-two-dimensional, single particle, and equivalent circuit models are based on physics [22]. These models provide insights into electrochemical processes using differential equations, and circuit elements. These models vary in complexity and require extensive parametrization and re-parametrization at different health states. Electrochemical models can be more quickly parameterized using grey-box biology-inspired search algorithms [23]. However, these algorithms still require rigorous computation and can be difficult to implement onboard due to re-parametrization at different states. To expedite computation time, data-driven modelling using machine learning has become commonplace in LIB health diagnostics [24]. Machine learning algorithms front-load the model optimization in the training phase to make quick predictions on new data using the parameterized model. This can be used to conduct real-time health predictions or project future degradation. Machine learning can also decipher patterns from multiple sources of complex data acting as a useful tool when coupled with existing battery sensors [2]. These reasons make black-box modelling appealing for predictions related to battery health and show promise for online integration with battery management systems [25]. There are challenges with machine learning regarding data quality, quantity, and model acceptance [26, 27]. To combat these challenges, models should ensure data diversity and consider methods of enhancing model interpretability.

This thesis aims to apply machine learning algorithms to tackle challenges related to LIB degradation. The two tasks we have chosen highlight the variability of LIB degradation and showcase the importance of gaining information beyond standard capacity measurements. The first addresses the need for real-time prediction of EIS quantified degradation modes conductivity loss, loss of lithium inventory, and loss of active material. The second study employs this knowledge of degradation modes to sort retired LIBs based on their viability as a reused second-life battery. Our goal is to determine solutions to these problems while being mindful of model practicality. This involves selecting input data that is accessible and pragmatic for the selected task, along with providing model transparency.

1.3 Contributions

The contributions of this study follow our outlined objectives to apply rapid, interpretable, and easily implemented machine learning algorithms to relevant challenges in the LIB health monitoring field. We apply these objectives to two studies resulting in the following contributions:

1. Our first study explores the variability of degradation mode propagation through cycle life. A method of quantifying degradation modes using basic constant current and constant voltage charging features using a Random Forest algorithm is then implemented. Input feature importance is analyzed providing insights into regions of importance within these charging curves.

2. The second study develops a method for classifying lithium-ion batteries for second life using a one-shot EIS measurement approach. Data scarcity in second-life batteries is addressed using a variational autoencoder for dataset augmentation. The results of this model are discussed with uncertainty against a baseline method seen in real-world applications.

1.4 Agenda

This thesis has been organized into four chapters. Following the first introductory chapter, chapters 2 and 3 are co-authored manuscripts that will be submitted for publishing. There is a short preface for each of these chapters describing the role of the authors. The structure of this thesis is as follows:

Chapter 2 - Degradation Mode Quantification Using Machine Learning This chapter explains our data-driven method of quantifying EIS-determined degradation modes in real time using accessible data. This model is trained and tested using our in-house Molicel lithium-ion battery degradation data.

Chapter 3 - Data-driven Classification of Lithium-ion Batteries for Second-life Applications

This chapter explores the benefits of using EIS data to gain insights into future battery degradation. This method is applied to second-life Lithium-ion batteries to classify whether they should be reused or recycled based on initial EIS measurements.

Chapter 4 - Conclusions This chapter highlights our contributions and ensure the goals of this thesis are met. We also explore avenues for future work to expand upon this research.

Chapter 2

Lithium-ion battery degradation mode quantification using machine learning

This chapter is based on a manuscript that will be submitted to the Journal of Power Sources with the same title as this chapter, authored by L. Murphy and Dr. C. Crawford. The author L. Murphy was responsible for the methodology, data processing, modelling, analysis, and manuscript writing. Author Dr. C. Crawford was responsible for supervision throughout this study along with reviewing and editing the manuscript. Jules Pare and Sean Buchanan are also acknowledged for their work in the PRIMED battery lab gathering the data used in this manuscript.

2.1 Abstract

In this work, a method of quantifying degradation modes using accessible voltage and current data for Lithium-ion battery health analysis is presented. The degradation modes conductivity loss, loss of lithium, inventory, and loss of active material represent internal battery degradation mechanisms that lead to capacity and power performance decline. The degradation modes were quantified after fitting experimentally obtained NCA cell electrochemical impedance spectroscopy data to a second-order RC circuit model. A random forest algorithm was used to predict these parameters based on constant current and voltage charging times as the model input. The model was able to achieve R^2 values of 0.95, 0.98, and 0.91 when predicting degradation modes:

conductivity loss, loss of lithium inventory, and loss of active material respectively. The model's feature weighting was analyzed using Shapley values to determine the relative impact of certain areas of the constant current and constant voltage charging curves on degradation mode prediction. It was found that both constant current and voltage-based features had a significant impact on the model's prediction.

2.2 Introduction

Electrification of the energy and transport sectors is imperative to achieving ambitious climate targets set across the globe. This process hinges on the ability to store energy effectively due to spatial and temporal challenges associated with variable renewable energy resources, and end-use cases such as transportation. Lithium-ion batteries (LIBs) are a highly efficient and energy-dense method of storage that can be designed for a range of capacity and power requirements. The primary drawback of Li-ion batteries is the degradation they experience, which is accelerated by stress factors such as time, depth of discharge, C-rate, and temperature. LIB degradation is typically referred to as capacity loss, however, many internal chemical and mechanical degradation mechanisms can be grouped based on their effect on battery performance. These groups are referred to as degradation modes (DM) and are primarily described by: conductivity loss (CL), loss of lithium inventory (LLI), and loss of active material (LAM). CL is caused by the corrosion of current collectors and electrolyte decomposition, leading to power fade in the cell preventing it from running safely at its rated power and restricting use in specific applications [28]. LLI affects battery capacity via chemical side reactions. This can take place on the solid electrolyte interphase causing lithium to plate to the electrodes irreversibly, along with pore blockage [17]. Finally, LAM describes the deterioration of the electrodes through cracking, and structural disordering, resulting in both capacity and power fade. The correlations between stress factors, degradation mechanisms, degradation modes, and their effect on battery performance are visualized in Figure 2.1 [2, 3]. Understanding the trajectory of these degradation modes as the battery is cycled can help inform on the remaining useful life, safety, failure diagnosis, battery maintenance/replacement, and optimal system control. The proper operation and care of LIBs can help facilitate the use of these batteries in second-life applications, prolonging the technology's life-cycle and reducing its overall carbon footprint.

Pseudo open circuit voltage (pOCV) modelling is one of the most common ways

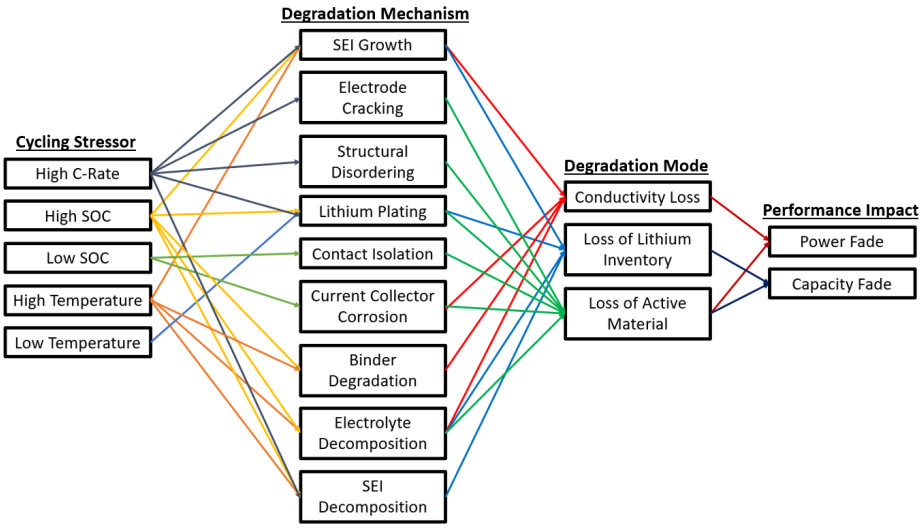

Figure 2.1: Battery aging stressors and their resulting degradation pathways, adapted from [2, 3]

to identify DMs. These techniques are referred to as incremental capacity (IC) and differential voltage (DV) analysis, where slow charging and discharging cycles are used to plot the rates of change in capacity in relation to the cell voltage and vice versa. The shifts and changes in the height of peaks on IC and DV plots can be attributed to LLI and LAM [29]. These methods require a pOCV measurement at the beginning of life and at the current state to assess the baseline and extent of degradation. While IC and DV methods can be useful for half-cell analysis to determine the loss of active material on both the cathode (LAMp) and anode (LAMn), they also have their drawbacks. pOCV-based methods have difficulty determining conductivity loss, so they are commonly excluded from analysis as it is not the most dominant DM [29]. pOCV measurements are also usually conducted at currents of less than 1/20C, which is often impractical in real-world applications [29, 30]. Implementations of DV and IC for DM analysis can be found in the following papers [31, 32, 33].

Another testing method used to assess internal battery dynamics is Electrochemical Impedance Spectroscopy (EIS). EIS is a technique used to assess battery impedance by imposing an AC potential over a range of frequencies. EIS readings are traditionally used to fit the components of an equivalent circuit model (ECM) for battery simulation, control, and monitoring [34]. Adaptations of the Randles Circuit Model are used to model Li-ion cells and contain resistor components labelled, R_{bulk}, R_{sei}, R_{ct}, and $R_{Warburg}$ (R_w) [20]. These resistors are named based on their respec-

tive role in the cell, R_{bulk} associates electrolyte, separator, and electrolyte resistance, R_{sei} refers to resistance in the solid electrolyte interphase layer, R_{ct} refers to charge transfer resistance, and R_w is attributed to the diffusion resistance in the electrodes [20]. Pastor-Fernandez et al. (2016) propose that the ECM resistance parameters R_{bulk}, R_{sei} + R_{ct}, and R_w have the strongest correlations with degradation modes CL, LLI, and LAM respectively [28]. Pastor-Fernandez et al. (2017) validate this method with proven IC and DV analysis [35]. Pastor-Fernandez highlight the limitations of ECM-based DM quantification as the ECM parameters may represent a combination of DMs when this method only attributes the ECM parameters with the most pertinent DM. Sun et al. furthered this method by investigating the effects of SOC, current, and other ECM architectures on DM quantification using EIS [36]. It was discovered that measurements taken at low SOCs can result in DM overestimation with the exception of CL. EIS has advantages in the speed of measurement, but EIS equipment is expensive and is traditionally only used in a laboratory setting. ECM-based DM quantification also experiences disadvantages in its accuracy, as the model parameters may represent a combination of DMs.

Another method that can quantify battery internal resistance is Hybrid Pulse Power Characterization (HPPC). HPPC testing injects high current pulses at various SOCs and assesses the instantaneous voltage jump/drop. Duru et al. use HPCC testing to identify ECM parameters, leading to battery simulation voltage accuracy within 0.5% of experimental results [34].

Both of the aforementioned DM identification techniques rely on time-intensive modelling or post-processing for the computation of DMs. Currently, this space is being advanced and made more practical with the use of data-driven models. There are numerous articles in the literature regarding SOH prediction for LIBs using various model inputs. Zhang et al. use impedance data from EIS measurements as an input to predict battery SOH and remaining useful life through a Gaussian Process Regression [4]. Field-accessible data inputs such as current and voltage are favoured due to their ability to integrate with battery management systems (BMS). Shu et al. conducted a review of the SOH prediction models and highlighted the many different input features that can be used [37]. Lin et al. use the constant current charging time as an input feature to predict capacity using a random forest regression, and they achieve R^2 values upwards of 0.95 [38]. Ruan et al. implement a convolutional neural network equipped with change in the capacity as a function of voltage as input and

DMs identified through IC analysis as the output [39]. This is a great improvement to the IC method with DM quantification in under a second. Xu et al. use ensemble learning to identify pOCV-accessible degradation modes LAMp, LAMn, and LLI [30]. This model uses the current equivalent cycle number as the model input along with various operating conditions such as peak discharge current, minimum discharge current, peak voltage, minimum voltage, temperature, charge/discharge current, and cut-off voltage. These data-driven methods of recognizing DMs can be applied using BMS-accessible data with significant pre-processing, and/or prolonged charge and discharge cycles. Li et al. implement this by using field-accessible measured current and voltage data from both high and low dynamic cycling profiles as input to a cuckoo search algorithm to predict DMs quantified through IC analysis [40]. Similar to the HPPC testing method, highly dynamic cycling profiles provide resistance information through voltage drop/jump. This is a large improvement to current DM quantification methods as this has a low barrier of entry to be applied in real-world systems. A typical BMS monitors the voltage and current at both the pack and cell level to ensure cell charges are balanced [41].

To address some of the previously discussed areas for improvement in DM analysis, we propose a method for DM quantification using data-driven modelling, field-accessible input data, and minimal data processing. Field-accessible data refers to data that may be readily available during normal system operation. This paper provides consideration of the practicality of machine learning methods for battery health assessment by using easily accessible data from a typical BMS. The effect of the input features on the model performance is also investigated in an effort to provide model explainability. The progression of DMs, (CL, LLI, and LAM), in high-power NCA cells is discussed along with the effect depth of discharge (DOD) and C-rate have on these modes. The primary contributions of this paper are summarized as follows:

1. Investigated the effect of depth of discharge and C-rate on the degradation mode progression on Molicel batteries over a year-long testing period with intermittent EIS testing, resulting in approximately 2000 equivalent full cycles per cell.

2. Multiple easily implemented machine learning methods are compared in their ability to predict degradation mode pathways using field-accessible voltage and current data.

3. Input feature importance is explored through the use of Shapley values to provide insights into constant current and constant voltage charging times impact across target DMs.

The remainder of the paper is divided into four sections that include, methodology, results, discussion, and conclusions. Section 2 describes the methodology including experimental setup, data acquisition, model framework, data processing, and model selection. Section 3 covers the DM increase over the testing period for each cell, tabulates and plots our DM prediction results, and provides insight into the model decision-making through Shapley values. Section 4 discusses the significance of the observed results along with the potential for future work and model improvements. Finally, section 5 summarizes the results and findings.

2.3 Materials and Methods

2.3.1 Data Acquisition

The data used in this study was obtained from the Pacific Regional Institute for Marine Energy Discovery Battery Lab. Battery specifications are given in Table 2.1 [42].

Table 2.1: Cell type and manufacturer specifications.

Name	**Chemistry**	**Size**	**Nominal Capacity**	**Nominal Voltage**	**Lower Cut-off Voltage**	**Upper Cut-off Voltage**
Molicel P42A	NCA	21700	4200 mAh	3.6V	2.5V	4.2V

The cells in this experiment were cycled in a Thermotron S-8-8200 environmental chamber using an Arbin LBT 5V-60A, 16-channel, battery testing unit. The Arbin LBT measures voltage, current, time, capacity, energy, resistance, and temperature. The cell testing was broken into two main periods: degradation and characterization cycling. The majority of the testing period consisted of degradation cycling wherein the cells were repeatedly cycled at various DOD from 100-X%, and constant C-rates at an elevated temperature of 35°C. Characterization cycles took place every two weeks to determine the current health status of the battery. This involved ensuring

an ambient temperature of 23 °C, conducting charge and discharge cycles at 0.33C, and EIS impedance measurements. Characterization charging cycles consisted of two sequential phases, constant current (CC), and constant voltage (CV) charging. CC charging was performed at 0.33C (1.32A) between 2.5 and 4.2V; once the cell reached 4.2V, CV charging began and the current was tapered until it reached 0.04A at termination. The EIS measurements were conducted using a Gamry Interface 1010E potentiostat over a frequency range of 1 Hz to 100 kHz. EIS operates by delivering an AC potential at a number of different frequencies and measuring the phase difference of the battery's current response [20]. This experiment continued for either 1 calendar year or until the cell reached 70% SOH and was retired. The independent variables in this experiment were DOD and discharge C-rate while the charging current remained constant at 1C between tests; Table 2.2 shows the breakdown of each cell's assignment.

Table 2.2: Testing conditions for each cell.

Cell Number	**Depth of Discharge (%)**	**Discharge C-rate (C)**
Cell 1	40	4
Cell 2	80	1
Cell 3	80	2
Cell 4	40	1
Cell 9	80	2
Cell 10	40	4
Cell 11	80	4
Cell 12	40	2
Cell 13	80	1
Cell 14	40	1
Cell 15	40	2
Cell 16	80	4

This data was selected due to the variety in discharge depth and discharge C-rate, which should ultimately lead to differing degradation pathways. It is of interest to analyze the resulting capacity fade and degradation mode propagation under these different conditions. Repeated cycling conditions allow for analysis of cell to cell DM variability. Characterization cycles occurred every two weeks throughout cycling, resulting in approximately 180 unique EIS measurements over varying battery states of health.

2.3.2 Model Framework

Having collected all of the relevant data from the Arbin LBT and Gamry EIS units a model framework is proposed. The framework can be divided into sections as shown in Figure 2.2 including data acquisition, data processing, training, and validation.

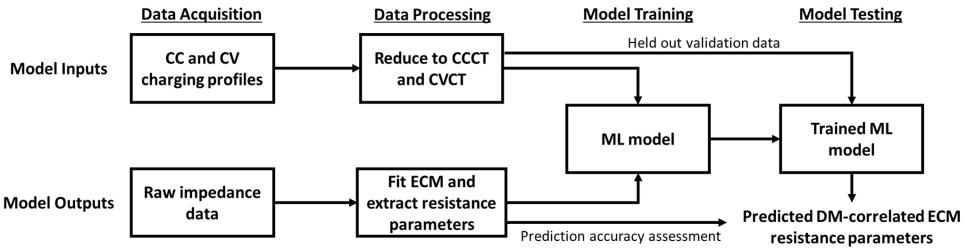

Figure 2.2: Graphic of the battery degradation mode quantification framework.

2.3.3 Data Processing

Input Data

To effectively predict DMs using machine learning, a set of input features that correlate with the battery's internal dynamics was selected. Extracting time-based features from constant current and voltage charging profiles can provide insights into the capacity and power fade. Feature extraction is crucial in machine learning with smaller datasets as large complex time series inputs can be difficult to decipher with few true output observations. In this case, domain knowledge is used to distill long charging curves into lower-resolution time features. Three time-based health features were extracted from the CC and CV charging profiles to act as model inputs:

1. The constant current charging time (CCCT), defined as the time to charge at CC between 3.8 and 4.19 V;

2. The constant voltage charging time (CVCT), the time to charge at CV until I < 0.04 A;

3. The sum of features 1 and 2.

The CCCT is as an effective feature for SOH prediction that enables distinguishing DMs associated with capacity fade [38, 43, 44]. The CCCT decreases as the cell's capacitance decreases, and resistance increases. As outlined by Bhatt et al. this

corresponds with the voltage drop across the SEI layer, and available lithium in the cathode [43]. The second feature, CVCT, is a weak indicator of battery SOH. However, its relation with the insertion of lithium-ions in the anode may be useful for identifying an increased resistance. A prolonged CVCT may be an indication of difficulty accepting charge, as the current is tapered based on the cell voltage's proximity to the charging voltage. The third feature sums CCCT and CVCT serving as an indicator of the total charging time (TCT). While the capacity of the cells decreases with degradation the TCT tends to increase as more time is spent tapering current in the CV phase. This was found to help make DM predictions as it aids in relating the changing CC and CV phases. Incremental capacity analysis uses changes in peak capacity rates of increase with respect to voltage as an indicator of DM propagation. Changes in the charging times in the CC and CV phase are a result of these peaks shrinking and should show strong DM correlations. This effect can be observed in Figure 2.3 depicting the CC and CV charging modes throughout cell 16's life.

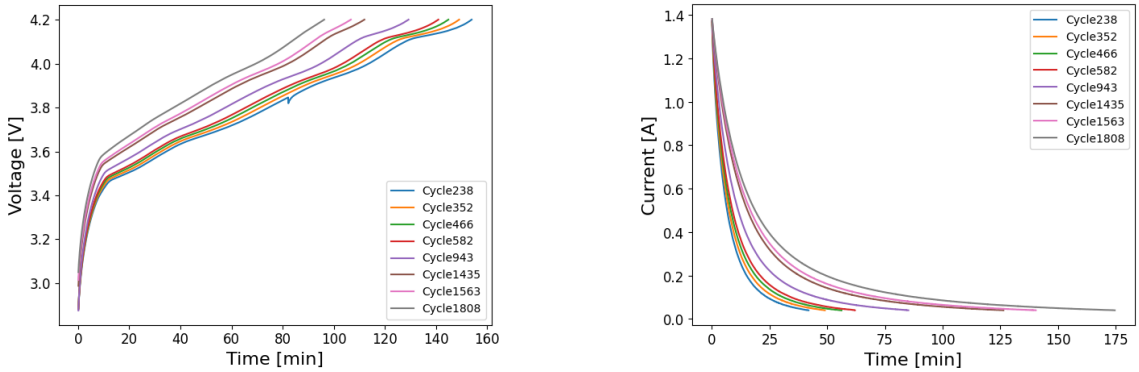

(a) Constant Current profile.

(b) Constant Voltage profile.

Figure 2.3: CC and CV charging profiles for each characterization cycle of cell 16's lifetime, labelled by equivalent full cycle number in the legend.

Output Data

The collected EIS data was used to fit the parameters of an equivalent circuit model (ECM) representation of the cells. Firstly, the EIS data was filtered to ensure all measurements were conducted at approximately 23 °C. Characterization cycles that did not occur at 23 °C were excluded from the dataset, as ambient temperature has a strong relationship with cell resistance. This occurred due to an issue with syncing each cell's characterization test and resulted in data from cycles between

approximately 250 and 1250 being removed for some cells. The EIS data is fitted to the ECM using the non-linear least squares method integrated into the impedance.py Python package [45]. Using an iterative approach various ECMs were tested and evaluated based on the root mean squared error between the fit and actual data. Common ECMs used for Li-ion battery modelling were tested, such as the Randles and CPE Randles circuits, along with customized versions of these circuits. The best fit was found to be a modified Randles circuit shown in Figure 2.4, and the resulting values were assessed visually and cross-referenced with existing literature [28, 46]. Further information on ECM fitting can be found in Appendix A.

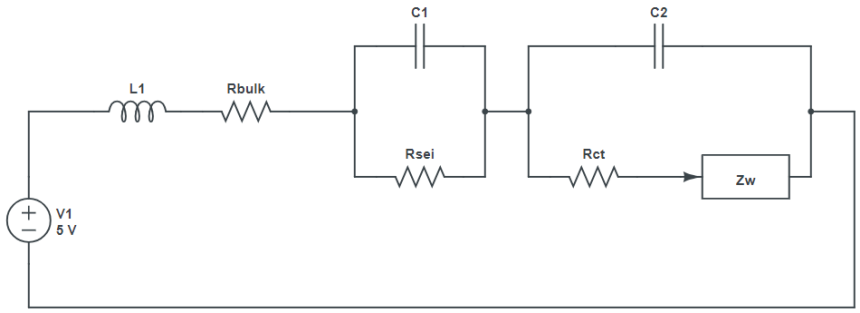

Figure 2.4: Modified Randles equivalent circuit model.

The ECM parameters are then used to assess the degradation mode pathways over the cell's lifetime. As identified by Pastor and Fernandez changes in R_{bulk} correspond with CL, R_{sei} and R_{ct} are primarily determined by the LLI, and Z_w changes with the LAM [28]. The Warburg impedance Z_w is a complex value that is expressed as $R_w + i_b$. The Warburg resistance R_w represents the diffusion resistance in the battery. The model is set to predict ECM resistance values for R_{bulk}, R_w, R_{sei} and R_{ct} as DM indicators.

The impedance increase for each degradation mode is computed between the first and last characterization cycle of the experimental period. The impedance percentage increases over cycle life across high to low-frequency processes allows for comparison of internal degradation between different cycling conditions. This is conducted using Equations 1-3 [28, 47].

$$CL\% = \frac{Rbulk_{\mathrm{i}} - Rbulk_0}{Rbulk_0} \tag{2.1}$$

$$LLI\% = \frac{(Rsei_{\mathrm{i}} + Rct_{\mathrm{i}}) - (Rsei_0 + Rct_0)}{Rsei_0 + Rct_0} \tag{2.2}$$

$$LAM\% = \frac{Rw_{\mathrm{i}} - Rw_0}{Rw_0} \tag{2.3}$$

A Pearson correlation matrix displays the linear correlations between the outlined input features (CCCT, CVCT, TCT) and model outputs (R_{bulk}, R_{sei} + R_{ct}, R_w). As shown by Figure 2.5 there are strong correlations between the input and output datasets, confirming that the selected features are appropriate.

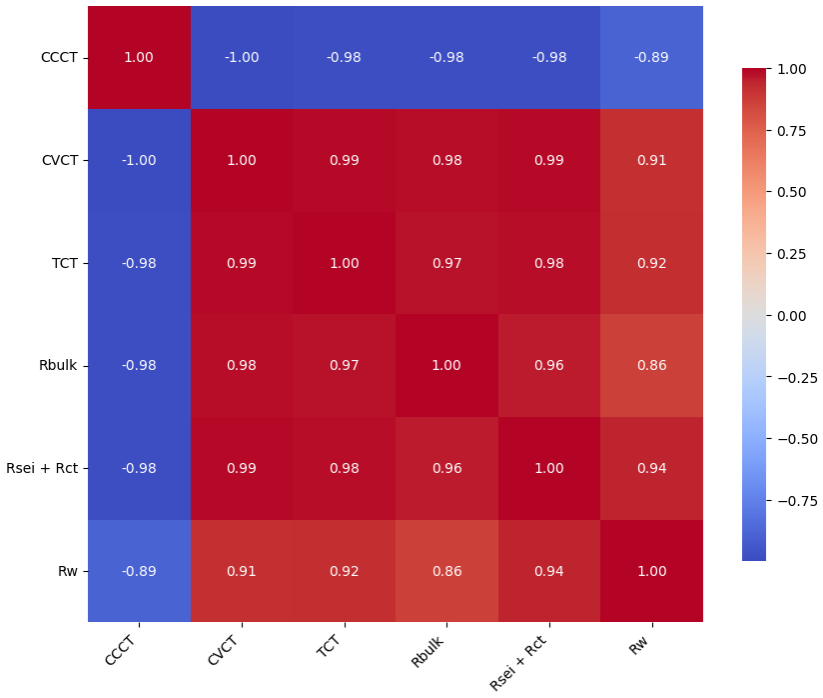

Figure 2.5: Pearson correlation matrix for input and output features.

2.3.4 Model Selection

Multiple data-driven models were evaluated based on the performance metrics mean absolute error (MAE) and R-squared. The models tested included: Linear Regression, Random Forest, Gradient Boost, K-nearest neighbours (KNN), and an Artificial Neural Network (ANN). The Linear Regression, Random Forest, Gradient Boost, and KNN methods were drawn from the sci-kit learn supervised learning package [48]. These models were fit using the multi-output regressor and tested using k-fold

validation. Multi-output regressors imply that the model outputs multiple variables instead of a single result. Native multi-output regressors such as Random Forest, and KNN, learn and predict all outputs simultaneously. Models such as Linear Regression, and Gradient Boost run multiple separate regressors in parallel. The sci-kit learn regression models require minimal hyper-parameter tuning, however, some key parameters were adjusted. The number of neighbours for the KNN algorithm was set to 6, and the maximum tree depth was set to 5 for the random forest through iterative tuning. The ANN is constructed using the Keras Python library and was the only deep-learning model evaluated. This network used 3 inputs to predict 3 outputs and used one dense hidden layer with 64 units.

These models were selected based on their ease of implementation, computation time, ability to work with smaller datasets, and diversity in the optimization approach. Data-driven modelling approaches can suffer from over and under-fitting when dealing with relatively small datasets, so combating this issue was the main consideration in model selection. Overall model performance was monitored using held-out test data. This helped prevent unnecessary complexity and avoid overfitting to the training data, so that model predictions maintained generalizability. The data was scaled between zero and one due to the differing magnitudes between features to reduce bias in the training process. Under-fitting occurs when the model is overly simplified and cannot learn the trends and intricacies of the training data. To combat this, models with varying optimization processes were chosen to determine which would best fit this specific task.

The Linear regression model acts as a baseline for this analysis, as it simply fits a linear function to the data, which typically underfits complex data [49]. The random forest and gradient boosting models are methods of ensemble learning using decision trees that average results across multiple trees to prevent overfitting. The KNN is chosen as it performs well with low-dimensional data and operates by recognizing simple patterns between localized information. Lastly, an ANN is tested to determine if a more complex network is required to discern a relationship between model inputs and outputs.

2.4 Results

The results of this study focus on understanding why the prominent DMs are changing as the cell ages, the ability to predict this trajectory, and visualizing how these predictions are made. We start by looking at the percentage increase of each DM in the cells to discuss their correlations between DOD and C-rate. Next, the prediction accuracy of the selected machine-learning models are compared, and the results of the elected model are plotted. Finally, the weighting of each input feature on the DM prediction is determined using Shapley values to add model explainability.

2.4.1 Data Analysis

The results of the degradation mode analysis using equations 1-3 show that even under the same cycling conditions degradation modes may propagate differently from cell to cell. This is depicted in Figure 2.6 by cells 4 and 14, 1 and 10, and 11 and 16. The data also shows that increasing the depth of discharge has a much greater effect on cell degradation than the discharge C-rate. This can be partially attributed to Molicels being designed to discharge at C-rates of up to 10C [42] and therefore may see more exaggerated degradation closer to the limit. The increased depth of discharge yields approximately double the capacity loss over the same number of equivalent full cycles, however, the DMs do not necessarily follow the same scaling. This demonstrates a need for a model that can provide rapid DM predictions using accessible data over a range of degradation states.

It is interesting to note that the relative DM propagation of CL in the 40% DOD cells is much higher than in the 80% DOD cells. This can be attributed to the fact that LAM is primarily affected by SOC, while CL is affected by high current rates [36, 17]. LLI and LAM being observed as the dominant DMs concurs with previous studies [36]. Whether LLI or LAM is more dominant appears to be somewhat random in the 40% DOD cells, as opposed to the 80% DOD cells. In the 80% DOD cells, both of the 4C discharge rate cells manifest LAM as the most dominant DM. LAM also tended to propagate later in cycle-life as depicted in Figure 2.10. This may indicate that while these pairs of cells appear to be at a similar 'state of health', those with higher LAM would be negatively affected in the future. The knee point phenomenon is defined as a rapid increase in the capacity loss rate due to a build-up of degradation mechanisms within the cell. This is primarily brought on by SEI damage, Lithium-plating, and

loss of active materials, making degradation modes a promising knee-point indicator [50]. Revealing deeper insights into battery SOH with DMs may help with sorting batteries at the end of life, but also will help ensure safe operation during a more volatile period of life. Comparing cells 16 and 1, while 16 has experienced double the capacity loss it also has experienced over 20 times the impedance increase for LAM and over 10 times for LLI. This suggests that this cell will likely experience failure and should be monitored closely regardless of the SOH reading. A difference like this is drastic and could be as simple as the result of the battery owner's charging habits.

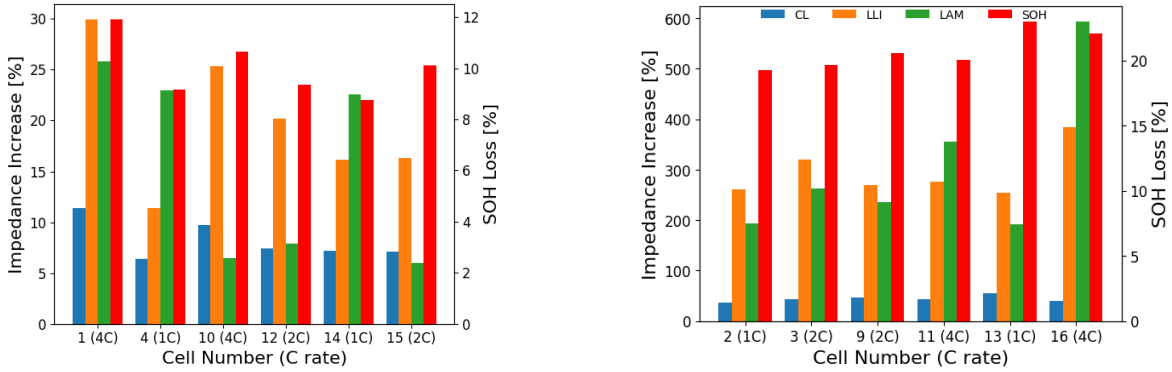

(a) Cells cycled at 40% DOD.

(b) Cells cycled at 80% DOD.

Figure 2.6: The percentage impedance change for each degradation mode and state of health loss between the first and last recorded characterization cycle. Subplots for different DOD of degradation cycles.

2.4.2 Model Evaluation

Several data-driven models were compared to see which would yield the best result against scoring metrics R^2 and MAE. The R^2 is a strong, scale-agnostic method of assessing the performance of regression tasks. The R^2 value denotes the percentage of variance in the data captured by the model. This suits our task as we explore the variance in degradation modes through cycle life. MAE is also calculated as a supplementary metric for comparing prediction accuracy between the tested models. These performance metrics are defined as [51]:

$$R^2 = 1 - \frac{\sum_{i=1}^{n}(y_i - \hat{y}_i)^2}{\sum_{i=1}^{n}(y_i - \bar{y})^2} \tag{2.4}$$

$$MAE = \frac{\sum_{i=1}^{n}(\hat{y}_i - y_i)}{n} \tag{2.5}$$

n = Number of data points
y_i = Observed values
$\hat{y}_i$ = Predicted values
$\bar{y}$ = Mean of the observed values

The model is tested by leaving 3 cells (25%) out of training at a time and repeating the training process 4-times for various cell groupings, known as k-fold cross-validation [52]. The groupings are referred to as batches from 1-4 respectively that include cells (1,3,16), (2,4,10), (9,11,14), and (12,13,15). This procedure allows for model evaluation across the whole dataset. The performance metrics are averaged across each test batch for each DM and are compiled in Table 2.3 to reveal the model best suited for this task.

Table 2.3: Comparing testing accuracy from different machine learning models based on performance metrics R^2 and MAE.

Model	**MAE CL**	**MAE LLI**	**MAE LAM**	**R^2 CL**	**R^2 LLI**	**R^2 LAM**
Linear Regression	0.043	0.038	0.055	0.94	0.96	0.76
Gradient Boost	0.041	0.031	0.037	0.94	0.97	0.85
K-Nearest Neighbours	0.041	0.031	0.035	0.95	0.97	0.88
Random Forest	**0.039**	**0.030**	**0.034**	**0.95**	**0.97**	**0.89**
ANN	0.042	0.031	0.037	0.94	0.97	0.87

Table 2.3 shows that the Random Forest yields the strongest test results for this task. Gradient Boost and Random Forest are examples of ensemble learning methods which aggregate predictions over multiple models. This helps reduce overfitting and increase generalization making these models suitable for seeing new degradation pathways moving forward [49]. Random Forest reduces error across all outputs simultaneously during training making it a strong multi-output regression model. While this model performs best over all of the DMs, it is important to note that all the tested models performed well including the linear regression. As highlighted previously with the Pearson correlation matrix this shows a strong linear trend between

the input and output features.

In an effort to improve our results, we can investigate further feature engineering. The chosen features are selected by segmenting our charging periods to reveal more detailed changes in charging dynamics. We decided to divide these phases into 4 segments, splitting the constant current charging curve into intervals:

$$T_{3.8-4.19V} = t_{3.8-3.91V} + t_{3.91-4.01V} + t_{4.01-4.12V} + t_{4.12-4.19V}$$

The constant voltage charging period is also segmented into 4 regions from 1.4 to 0.04 Amps:

$$T_{1.4-0.04A} = t_{1.4-0.35A} + t_{0.35-0.14A} + t_{0.14-0.07A} + t_{0.07-0.04A}$$

These regions are selected as they are equal time segments at the beginning of life, representing 25% of the charging time in this period. We utilize Shapley values to investigate the effect of these added features.

2.4.3 Shapley Analysis

One of the largest downsides to data-driven modelling is its black-box nature. To address this limitation, Shapley values are computed to better understand the model's decision-making, and weighting of certain features. Shapley values have the potential to optimize machine-learning algorithms and data collection in the battery space by advising on what data is useful. This can be especially useful for paring down features which opens up models that struggle with high dimensionality.

Shapley values were developed in the field of game theory for measuring the value of each player in a game and assessing their expected payout based on the player's contribution [53]. In machine learning, this method is applied to assess the impact of each model input feature. In this experiment, Shapley values are calculated by evaluating the model performance for each permutation of input features, and then determining how each feature impacted the results using Equation 2.6 [54].

$$\phi_i(f_j) = \sum_{X \subseteq N \setminus i} \frac{|X|!(|N| - |X| - 1)!}{|N|!} [f(X \cup i) - f(X)] \tag{2.6}$$

ϕ = Shapley Value

i = Input Feature Number
j = Output Variable Number
f = Model
N = Represents all features
X = Subset of N

This process can be computationally expensive for machine learning models. The Tree Explainer feature of the SHAP Python package was used to conduct this analysis and visualize the results of the RF model [55]. The Tree Explainer leverages the structure of the tree models by following branches from the root to the leaf node determining the influence of each feature along the path. Lundberg et al. provide a detailed algorithm for this process [55].

SHAP values are commonly visualized using a Beeswarm plot as shown in Figure 2.7a. The Beeswarm plot displays the calculated SHAP value for every training data sample over each feature. The points are plotted along the x-axis based on their impact on the model output; those on the right and left contribute by either raising or lowering the prediction respectively. The vertical spread in the y-axis represents SHAP values where multiple input feature values fall. The points are colour-coded based on the sample's numerical value allowing for inference on which period of the battery's lifetime is most influential for certain predictions. This process is conducted for the multi-output regressor and the results are displayed in Figure 2.7. We can see a general trend that higher values of CVCT and TCT are impactful on larger DM predictions, while the opposite is true for the CCCT. This aligns with the Pearson correlations as CVCT and TCT grow as degradation ensues. The bar plot in Figure 2.7b shows the average absolute SHAP value for each of the input features. This indicates that when predicting all three DMs together, the latter portion of the CC curve and the beginning of the CV curve are most important. The non-overlapped Beeswarm plot for each DM can be found in Appendix A.

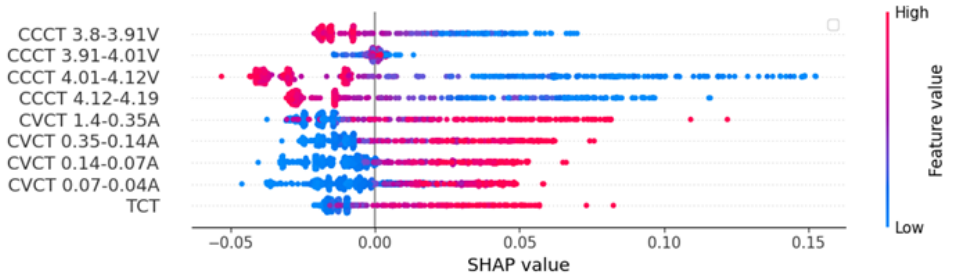

(a)

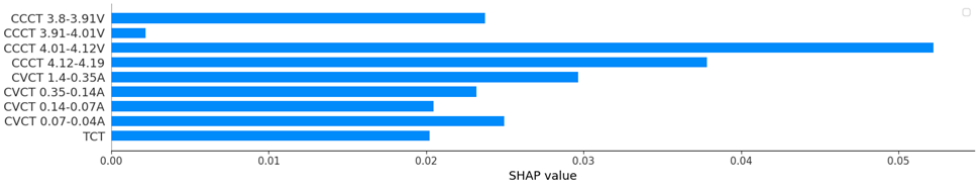

(b)

Figure 2.7: (a) Beeswarm plot of each input feature impact on the model output based on the magnitude of the feature value. (b) Average absolute magnitude of SHAP values for each input feature.

The bar graph in Figure 2.8 illustrates the impact of each input feature by showing the magnitude of the average impact on the model performance. The bar graph is a great method for visualizing the input's relative impact on each output feature. Figures 2.8a, b, and c represent the mean absolute SHAP value for each input feature on the respective DMs CL, LLI, and LAM. These were plotted using single-output trained models to determine any discrepancies in behaviour when trained as a multi-output model.

Figure 2.8a illustrates that the latter portion of the constant voltage charging curve is the most influential feature on the conductivity loss predictions. A prolonged CV tail indicates difficulty reaching the target SOC. This could be due to poor ion transfer at lower currents as a result of conductivity loss.

In Figure 2.8b we can see that the total charging time and the initial portion of the constant voltage curve are most important. This shows that using times from both the CC and CV curves is a good indicator of capacity loss and SEI growth when the full CC region is not accessible.

Similarly to LLI, in Figure 2.8c we see that the early stages of the CV curve and TCT are most important, however, in this case there is a greater emphasis on the

TCT. It is also worth noting that the end portion of the CV curve was essentially obsolete to the LAM prediction model.

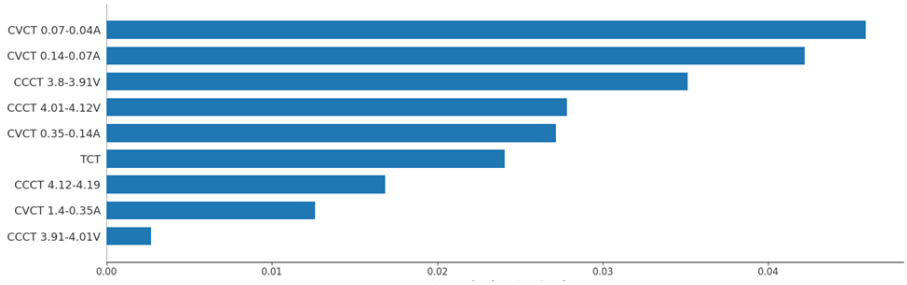

(a)

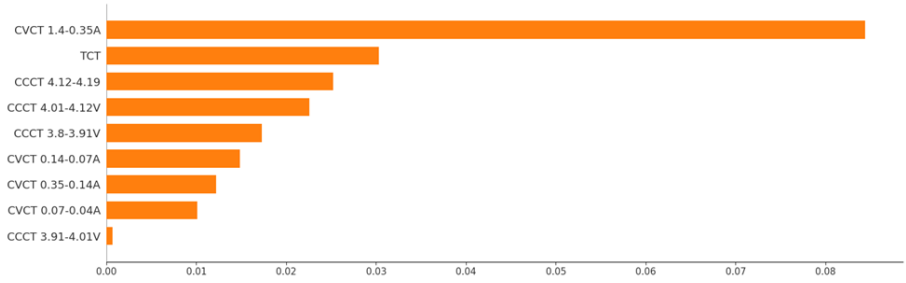

(b)

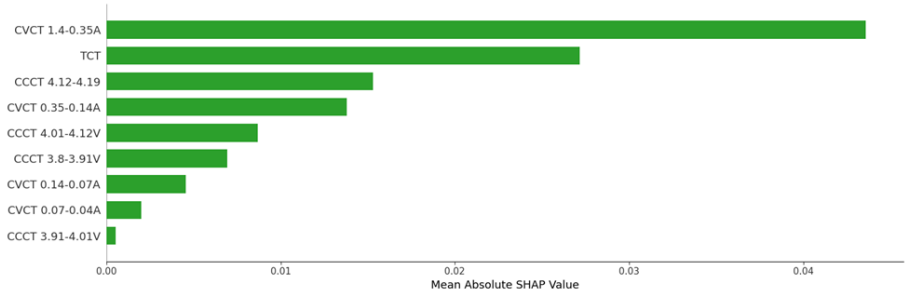

(c)

Figure 2.8: Bar graph of the mean SHAP value over all data representing each input feature's impacts on each degradation mode. (a) Conductivity loss. (b) Loss of lithium inventory. (c) Loss of active material.

Based on the evaluated Shapley values we pare down this larger feature set to the top three inputs. The feature set is reduced to not overcomplex the model with high-dimensional data, and have a fair comparison to the original feature set. Feature set refinement also eliminates potentially redundant, or unimportant features. We compare the results of different feature sets using their R^2 and MAE values averaged across each test batch. Feature set 1 includes the CCCT (3.8-4.19V), CVCT

(1.4-0.04A), and the TCT. Feature set 2 is refined by Figure 2.7, and composed of the constant current charging times between, $t_{4.01-4.12V}, t_{4.12-4.19V}$, and the constant voltage charging time between $t_{1.4-0.35A}$. The third feature set takes the top three features from the single output models shown in Figure 2.8. These features are applied to separate random forest models that predict an individual DM. The CL feature set contains the CVCT between $t_{0.14-0.07A}, t_{0.07-0.04A}$, and the CCCT between $t_{3.8-3.91V}$. The LLI feature set contains the TCT, CVCT between $t_{1.4-0.35A}$, and the CCCT between $t_{4.12-4.19V}$. The LAM feature set is identical to that of the LLI set. The heat map below in Figure 2.9 highlights the impact of each feature set on the model performance:

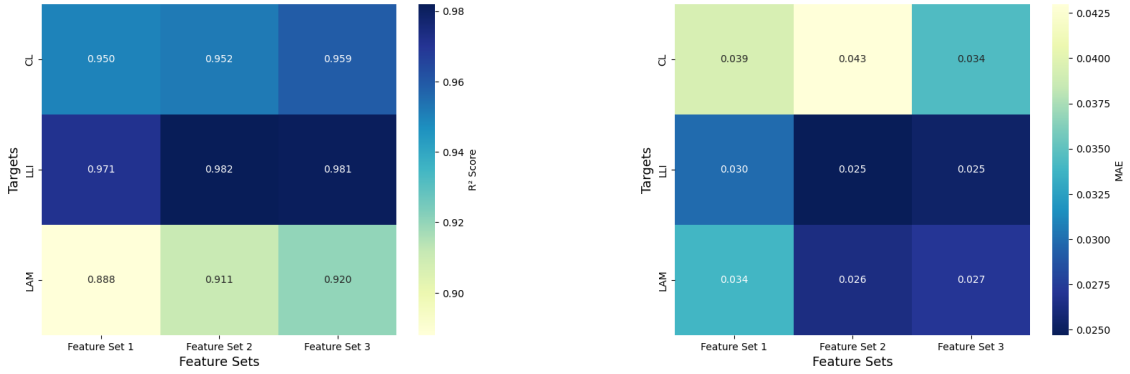

(a) R^2 (b) MAE

Figure 2.9: The performance of the random forest model given each of the outlined input feature sets.

The model was successfully improved using the refined feature sets. The multi-output Random Forest model using feature set 2 produced R^2 values of 0.95, 0.98, and 0.91 across DMs CL, LLI, and LAM respectively. This shows model improvement when feature refinement using Shapley values is employed. The model performance shows negligible deviation from Feature sets 2 to 3 for LLI and LAM predictions, however, it shows improvement for the CL target. This shows the importance of the elongated tail of the CV region for assessing CL and power fade.

The test results are visualized by plotting the predicted resistance values most correlated with each degradation mode, as shown in Figure 2.10a, while Figure 2.10b displays the de-normalized results of each test batch. The most significant errors appear to be under predictions at the upper boundary of the dataset. Tree-based models such as random forests have difficulty extrapolating beyond the feature space

due to the nature of its training regime [56, 57]. This is apparent in the final predictions of cell 16 in batch 1 as low-frequency impedance was rising rapidly, further sampling in this region may help remedy this issue. The linear regression model is better at extrapolating but is outperformed by the random forest overall. A decision tree visualization from the random forest training process can be found in Appendix A.

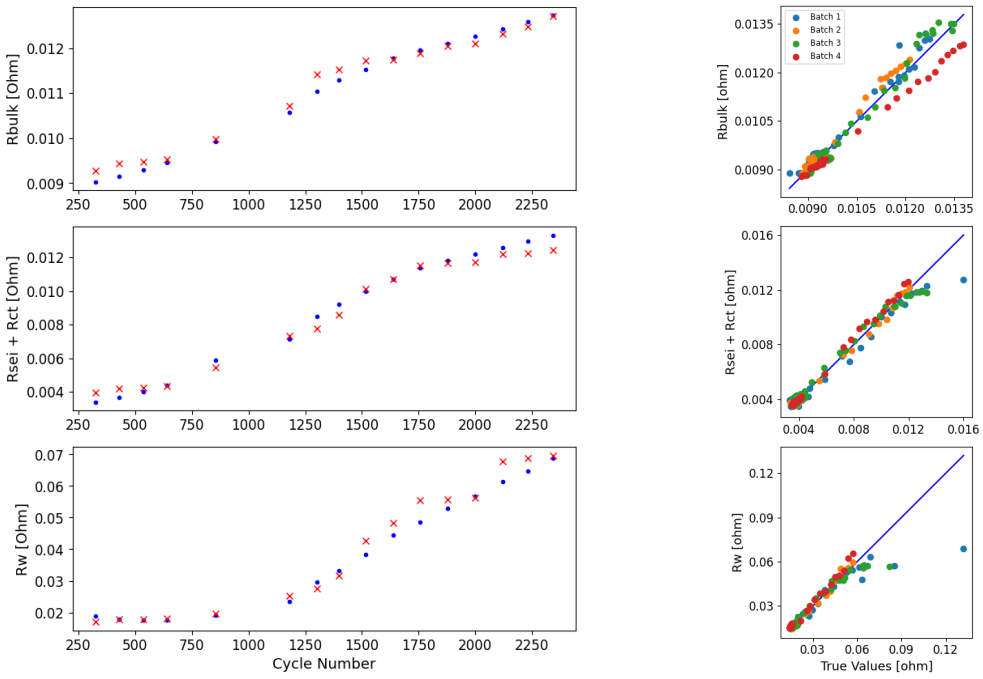

(a) (b)

Figure 2.10: (a) Degradation mode prediction with respect to characterization cycle number for cell 3. (b) All test results across batches 1-4 are plotted against the actual values.

2.5 Discussion

2.5.1 Results Analysis

This study has investigated the use of field-accessible experimental data to determine degradation modes in Lithium-ion batteries through the prediction of ECM resistance parameters. It was concluded that using a multi-output random forest regression algorithm could accurately quantify DMs, achieving R^2 values of 0.95, 0.98, and 0.91 when predicting CL, LLI, and LAM respectively. This method aligns with the

performance of existing SOH prediction models in the battery space as the results for CL, LLI, and LAM yield R^2 values upwards of 0.90 [4, 38, 58]. The R^2 value indicates that the model was able to capture over 90% of the DM variance over the cell's cycle life. The accuracy of the individual DM prediction may be improved by further tailoring separate models to each output feature, however, the goal of this project is to quantify pertinent degradation modes quickly with low computational cost.

2.5.2 Model Implementation and Significance

Optimization-based methods are commonly used for ECM parameterization and can achieve more accurate results by fitting the ECM to match battery operation. However, this process must be repeated at different stages of degradation, resulting in a computational challenge and making it difficult to implement online. Our method allows for quick predictions of degradation-affected ECM parameters by running real-time BMS data through a machine learning (ML) model trained over various degradation pathways. Full ECM parameterization can be applied for further battery modelling, which may be better suited to search algorithm-based methods. Using an ML algorithm to quickly propose strong initial values for crucial DM-correlated parameters could improve the optimization process at new states.

These DM estimates provide the model user with a deeper understanding of the battery's state of health to make informed decisions on battery safety, optimal control, and performance moving forward. Abnormal DM propagation may serve as an indicator of impending battery failure. This method could have significant applications in the real world by pulling the most basic BMS data of voltage, current, and time, to track DM trajectories. While this experiment had the characterization charging periods take place at 0.3C, it can be assumed that at higher charging rates the same effect on the CC and CV time periods is observed so long as each recorded charge is at the same temperature/C-rate. This is shown with the Oxford dataset as their characterization charging cycles were run at 1C and exhibited the same behaviour as the cell aged [38]. With typical charge rates for electric vehicles being around 0.5C, this method should be more applicable than comparative OCV-based approaches [59]. Using the charging times over different charging segments allows us to discern degradation modes using lower-resolution, and higher C-rate data. Instead of analyzing the incremental capacity changes, the charging times capture the effect

these changes have on cell charging behaviour. To add input feature accessibility the constant current period is set between 3.8 and 4.2 volts to account for the fact that batteries are not commonly fully discharged. The CV period is also considered readily accessible as electric vehicles typically undergo CC-CV charging [60, 61]. The CV or a similar current tapering period is required to ensure a smooth approach to the target SOC to assure no over-voltages and minimize aging.

2.5.3 Future Work

Future work on this study includes exploring methods of increasing the amount and diversity of the degradation pathways. This would include cycling at higher C-rates, a broader range of DODs, altering the degradation cycle temperature, and reaching lower SOHs. Previous studies have integrated the use of synthetic data to create many different aging pathways, along with ensuring there is a large amount of data [39]. A larger dataset would allow for deeper neural networks, higher dimensional data, and more complex time-series analysis to be explored which can result in higher model accuracy.

It is also recommended that this method is tested on another battery chemistry to monitor degradation mode development. This is suggested as Li-ion batteries of differing cathode chemistry are designed and optimized for different use cases resulting in varying levels of cell resistance [62]. Implementing this method on other LIB chemistries may require changes to voltage ranges and current limits. Future work may explore the comparison of the direct model application to other battery chemistries, against a fine-tuned or independently trained model. With these adjustments, this method could be trialled by coupling with live BMS data to track DMs in real-time.

Chapter 3

Data-driven Classification of Lithium-ion Batteries for Second-life Applications

This chapter is based on a manuscript that will be submitted to an undecided Journal with the same title as this chapter, authored by L. Murphy and Dr. C. Crawford. The author L. Murphy was responsible for the methodology, data processing, modelling, analysis, pilot study, and manuscript writing. Author Dr. C. Crawford was responsible for supervision throughout this project along with reviewing, idea generation, and editing the manuscript.

3.1 Abstract

As degraded lithium-ion batteries proliferate from aging electric vehicles, we must develop methods of forecasting battery lifetime to increase profitability and safety in second-life applications. However, electric vehicle batteries are subjected to variable and generally unknown operating conditions that yield different degradation mechanisms, affecting their future health trajectory. We propose a data-driven method of classifying retired Lithium-ion batteries to determine whether they should be reused or recycled. This method only takes a few minutes of testing requiring one electrochemical impedance spectroscopy measurement. The model was tested across five different use cases where the classification boundary was adjusted accordingly, resulting in an average accuracy of 92%. The model was also trained and tested against

another independent dataset, achieving 90% accuracy. This method shows promise as a tool for lithium-ion battery repurposing companies to identify batteries that will likely exhibit rapid capacity degradation if repurposed to avoid expending resources on full battery re-certification.

3.2 Introduction

3.2.1 Climate and Context

Climate policies are pushing away from fossil fuels into a clean energy transition, leading to the rapid growth of the energy storage market. Canada is committed to achieving 100% zero-emission light-duty vehicle sales by 2035, that are almost exclusively powered by Lithium-ion batteries (LIBs) [5]. One of the greatest concerns with LIBs is their capacity degradation. While this is influenced by battery usage, most EV batteries will have insufficient range for the consumer at around 70-80% of their original capacity [63]. This means that over the next 20 years, the number of retired EV batteries will increase exponentially at 25% annually [64]. With recycling costs being prohibitively high and total life cycle emissions implications there is pressure on battery manufacturers and consumers to find ways to prolong battery life.

3.2.2 Second-life batteries

An opportunity for a new market is rising that reuses retired full batteries for less rigorous applications before sending them for recycling. These battery packs can be stacked in parallel to create high-capacity energy storage systems. This method of maximizing battery potential offers profit incentives for battery repurposing companies such as Moment Energy and B2U [65, 66]. Depending on the use case and condition, second-life batteries (SLB) may last an additional 5 to 30 years before reaching end-of-life (EOL) defined as 40% state of health (SOH) [67]. Montes et al. found SLBs to be profitable in an energy arbitrage application, however, there are challenges [68]. As LIBs enter later stages of life, their degradation becomes less predictable. When cycled beyond the "knee point", the rate of capacity fade accelerates significantly [15, 69]. This phenomenon is brought on by the propagation of internal degradation mechanisms that inhibit charge transfer and intercalation of Lithium ions [70][71]. Over time, this can cause heterogeneity between cells within the same

battery pack [72].

Many retired EV batteries with similar driving range will have been subjected to different driving schedules, charging routines, and climates. These factors all have a significant influence on the degradation mechanisms that develop within the battery [2]. The variance in degradation can cause economic and lifetime uncertainty. This shows that a method of determining whether a pack is viable for a second life beyond simply measuring its capacity is required. Martinez et al. conducted a study to determine the impact of different first-life cycling conditions on second-life degradation [73]. It was found that battery degradation did not slow down once put in second-life applications, and only cells that have not yet exhibited a knee point were considered worthy of re-use. Ideally, battery packs are assessed on the cell level and refurbished to create a homogenous battery. Lee et al. developed a framework to reconfigure battery packs for second life to reduce cell-to-cell variation [74]. They propose an initial screening of battery capacity to eliminate outliers, followed by a secondary screening measuring open circuit voltage, ohmic resistance, diffusion resistance, and diffusion capacitance, to group the remaining cells homogeneously. However, as outlined by Montes et Al. the cost of disassembling packs to the module and cell level costs over 5 and 7 times more than leaving the pack assembled respectively [68]. It is concluded that to appropriately categorize whether a retired battery should be reused or recycled we must be able to correlate its current health with its future degradation path.

3.2.3 Modelling

Articles in the literature use various methods of modelling degradation to gain insights into LIB remaining useful life. These models vary from empirical linear and exponential models [72][68], to physics-based [75], to data-driven [76, 77]. Data-driven methods have become increasingly popular in the battery degradation modelling space, due to their speed and flexibility. Data can be drawn from online battery management systems, or measurements can be performed offline, such as electrochemical impedance spectroscopy (EIS) [4], high-powered pulse characterization (HPPC) [78], and charging/discharging cycles [79]. With battery degradation varying greatly based on chemistry, temperature, and use case, machine learning has an advantage over numerical models due to its speed in parameterization.

The main challenge of using machine learning in this application revolves around the accessibility to data. Cycle testing is time intensive, especially to reach lower capacities resulting in seldom publicly available SLB datasets. There are a small number of tested cells for those that do exist. This can be troublesome for data-driven modelling tasks, as dataset diversity and quantity are imperative for model training. Dubarry et al [80] look to solve this issue by creating synthetic voltage curves with a variety of cell chemistries and modes of operation based on a combination of physical models and experimental data. Transfer learning can also be used to re-train models on smaller experimental datasets [81].

Another factor to consider when implementing machine learning models is acquiring appropriate data, and extracting key features to achieve good results. Jiang et al [82] use incremental capacity analysis to determine cell consistency within packs based on resistance and capacity. Ran et al [83] use a clustering model to group cells based on capacity, voltage, and resistance using HPPC testing as the model input achieving an accuracy of 88%. Based on the literature it is clear that input features that consider internal degradation mechanisms are necessary for deciphering variability in SLBs [84, 70]. In-operando battery characterization regimes that provide internal degradation insights may include HPPC, EIS, incremental capacity analysis, and differential voltage analysis.

The accessibility of the input data is also important when contextualizing a data-driven model's practicality. When forecasting battery degradation, the time required for battery characterization to yield an accurate prediction plays a large role in feasibility. Cueto et al [79] propose a classification and regression data-driven model to predict the remaining useful life (RUL) of cells that experience a knee point in first life. This model looks to improve the RUL prediction space by using fewer cycles than other articles in the literature [76, 85]. Cueto labels the cells based on short, medium, and long lifetime and classifies them using voltage curve features from the first 3 cycles, resulting in 88% classification accuracy [79]. Haris et al further improve upon this using only the first cycle to determine the number of cycles to the end of first life (80% SOH), the cycle and the SOH where knee point occurs. These outputs allow the model user to connect the dots and plot an accurate degradation curve of two linear regions prior to and post-knee point. The inputs to this model include the initial internal resistance, charging time, differential voltage analysis, and average charging current. Using a CNN, the projected degradation curve had an average MAPE of

1.76 across the test data [77]. Many of the datasets used in these methods show knee point onset between 85-95% SOH due to accelerated testing which is not always representative of battery degradation under real-world operation [86]. Zhang et al [4] curate a degradation dataset of cycled cells with EIS and capacity measurements taken every other cycle. Zhang et al created both an SOH and an RUL prediction model to assess battery health in first life with raw EIS data as the model input, requiring no cycling. A GPR model is used to highlight uncertainty, and an average R-squared value of 0.85 is realized across the test cells.

Based on the literature, points of importance are identified for establishing a framework for SLB assessment. Firstly, it is shown that SLBs exhibit much less predictable degradation trajectories than batteries in first life [72, 73]. This is influenced by the battery's operating conditions in first life as this affects the extent of internal degradation mechanism development. This shows that SLBs should not soley be evaluated based on SOH (EV range) or the number of cycles (odometer) but should instead use a degradation mechanism indicator. Secondly, the literature suggests that batteries should be grouped or separated based on their condition to mitigate heterogeneity in degradation [83, 82, 79]. Data-driven modelling has become a standard in this effort as they can quickly learn patterns from complex battery characterization data. Lastly, it is observed that there is a push to lower the testing and computational time required to characterize SLB RUL [79, 77, 4]. This includes using data augmentation and simulation to improve the data acquisition process for model training.

3.2.4 Proposal

For this project, we implement a method of quickly determining the long-term viability of SLBs to exclude those that will fail quickly. This LIB classification method is geared towards third-party battery repurposing companies. These companies must know the lifetime of their product to address safety, warranty, and economic concerns. The status of a retired EV battery is often unclear due to privacy of BMS data [87].

We propose performing a single EIS measurement to conduct a fast assessment on the prospective SLB. It should be acknowledged that this method is tested with cell-level data. EIS can be performed on the pack, module, or cell level by adjusting the current amplitude depending on the system's current limits [88]. Cells are connected

in series and parallel to increase capacity and voltage yielding a higher power system. Impedance adds directly in series and combines as the reciprocal of the sum in parallel. As the battery size is scaled up, the impedance should still reflect the battery health similarly to the cell level. Pack-level EIS also provides information on wiring and connection-based impedance giving more insights into loss of conductivity [89]. It is recommended that SLBs be left in their pack form and not disassembled to preserve the existing BMS and reduce costs for certification [68, 90]. Relevant degradation-correlated features are then extracted from the EIS measurements through ECM fitting. Some EIS hardware may have built-in software that can automate this process when provided with an ECM [88].

Next, this data is inputted into a data-driven binary classification model to determine whether the battery is fit for a second life based on the predicted RUL. The boundary between these two camps is user-defined, in this application, the model indicates whether the battery should be re-used or recycled. To achieve better model accuracy with less data, a variational autoencoder is trained to augment the experimental dataset. For comparison, the current battery SOH will also be tested to determine second-life viability. The SOH represents the driving range of an electric vehicle, the goal of this comparison is to show how judging a prospective SLB by its SOH may be misleading. The measurement speed between these two methods differs by hours, as an accurate reading of the batterys SOH requires a full charge cycle at a low C-rate, while EIS measurements take a few minutes. EIS does not require the battery to be at a specific SOC when measurements are taken allowing predictions to be made without using a battery cycler.

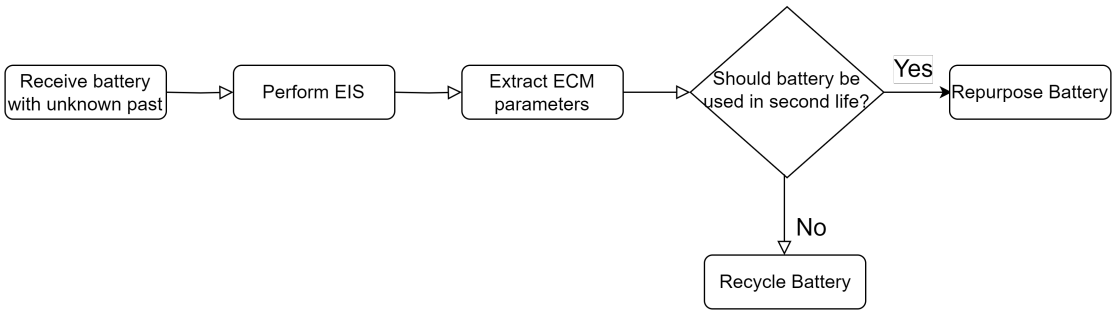

Figure 3.1: Retired battery sorting procedure.

The contributions of this project are:

1. Established a methodology for assessing battery viability for second life without cycling or past data.
2. Provided a framework for dataset augmentation through synthetic data generation in a data-scarce field.
3. The proposed method is compared to SOH-based sorting.
4. The model is validated with an independent second-life battery dataset.

3.3 Materials and Methods

This section outlines the datasets and extracted input and output features used for model training and testing to achieve objective one. We also describe our methodology for data augmentation to meet our second objective.

3.3.1 Datasets

Our SLB classifier was applied to two different second-life battery datasets, one public and one private. The publicly accessible Zhang dataset will be primarily discussed in this article [4]. The Zhang dataset consists of 12 45 mAh Lithium Cobalt Oxide coin cells. The cells are grouped by environmental temperature during cycling with 8 cells at 25 C, 2 at 35 C, and 2 at 45 C. Each cell is subjected to the same cycling conditions with EIS measurements taken every other cycle with a current of 5 mA and frequency range of (0.02-20 kHz).

For this study, we require cells that are cycled under the same conditions and pass the 80% SOH threshold to showcase the variability of RUL in second life. The naming convention by Zhang et al. is temperature followed by cell number, these cells include: 25C01, 25C02, 25C03, 25C05, and 25C06. The NREL data processing code was used for ease of implementation [91]. The capacity retention curves for these cells in second life are displayed in Figure 3.2, highlighting the volatility of SLBs.

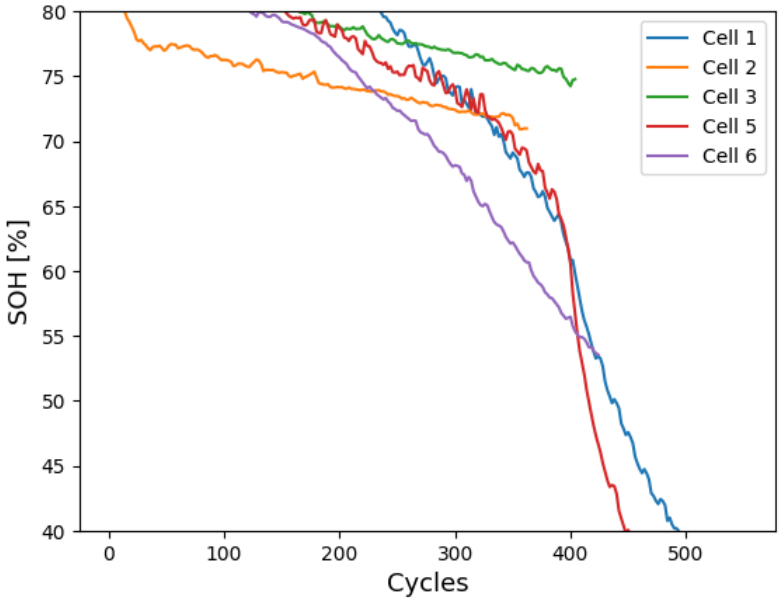

Figure 3.2: Capacity retention curves for cells cycled past 80% SOH in the Zhang dataset [4].

Pilot data is gathered to test EIS for SLB sorting on series and parallel connected cells. This data is made up of 4 first generation Nissan Leaf modules that consist of 4 cells each connected by 2 in series and 2 in parallel. Each module has an initial capacity of 66 Ah with a Lithium-Manganese-Oxide (LMO) cathode chemistry. These batteries were tested using the Pulsenics Pulse Probe 100, with a galvanostatic current amplitude of 0.5 A in a frequency range of 5-565 Hz [88].

3.3.2 Data Processing

Model inputs and feature extraction

A physics-based equivalent circuit model (ECM) of the batteries is built and parameterized using the acquired EIS data. Lithium-ion batteries can be modelled using the Randles ECM, which may be adapted depending on the battery chemistry. Similar to the process conducted in Chapter 2 an accurate ECM fit was found for this dataset through iterative testing with the circuit shown in Figure 3.3. Differing components include the substitution of constant phase elements for capacitors and the position of the Warburg impedance element. These changes are a reflection of the differing battery chemistry and EIS control parameters, which affect the impedance signature. Further information on the ECM fitting can be found in Appendix A.2.

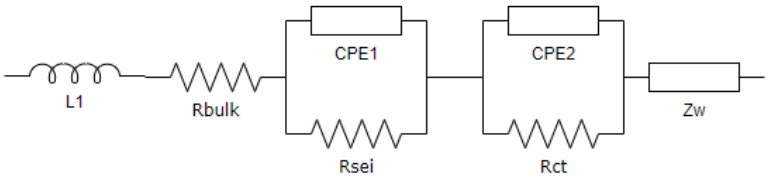

Figure 3.3: Optimal equivalent circuit model for LCO cells.

As shown in Figure 3.3 the resistors within the ECM represent different internal battery processes. Based on the effect they have on the battery ECM resistance parameters are grouped into the predominant degradation modes, conductivity loss (R_{bulk}), loss of lithium inventory ($R_{sei} + R_{ct}$), and loss of active material (R_w) [28, 20]. The state of these degradation modes is quantified in the EIS spectra with CL, LLI, and LAM corresponding to the high, mid, and low-frequency regions [17, 28, 36]. With this information, ECM parameters R_{bulk}, R_{sei}, R_{ct}, and R_w are chosen as the input features as they should be strong predictors of RUL in second life [70].

End of life and remaining useful life definition

As shown above, in Figure 2, second life has been defined as the area between 40 and 80% SOH following the literature [92, 67]. Due to SLB degradation variance, there are a small number of publicly available SLB datasets where all batteries reach the same EOL point. This requires an alternative method of quantifying a batterys RUL to the standard of counting the number of cycles to reach the EOL. In this work, the slope is computed from any point on the capacity retention curve to the EOL. Then, the slope is scaled based on the current SOH of the battery to account for those near EOL. This metric accounts for knee points in the future, current rate of degradation, and current capacity. This yields an appropriate method of assessing a battery without considering previous cycling. The equation for this calculation is provided below.

$$RUL = (1 - SOH_i) * \frac{SOH_n - SOH_i}{CYC_n - CYC_i} \tag{3.1}$$

Although this is a scaled degradation rate, for simplicity we will be referring to this as the RUL. A boundary is defined to classify a battery as reusable for a second life or immediate recycling with the calculated RUL metric. This can be a safety factor or break-even point that the model user defines to ensure batteries above a

certain rate of capacity fade are vetoed. RUL measurements are calculated at each whole SOH percentage between 60 and 80%. This yielded a dataset that spans the region of EV batteries that are likely to be retired [93]. This amounted to 20 data points per cell, and for cells that do not reach 60% SOH, additional samples are taken to ensure the dataset is balanced.

3.3.3 Model Architecture

Variational Autoencoder

As there are only five cells in the dataset data augmentation is explored. For this task, a variational autoencoder (VAE) generated synthetic data based on the experimental dataset while maintaining correlations between input features. This is a commonly used method in the machine learning field to create artificial data to augment, and balance smaller datasets [94, 95, 96, 97]. VAEs use a neural network structure to map the input data to a lower-dimension representation known as the latent space. The VAE is optimized using the sum of a weighted mean squared error and Kullback-Leibler (KL) divergence loss function. The mean squared error assesses the reconstruction of the experimental data, while the KL divergence loss encourages a Gaussian distribution through the latent distribution mean and standard deviation [98, 99]. Definitions for these loss functions are found in equations Appendix A.2.2.

After compression, a latent vector is passed through another neural network to be decompressed and produce a generated sample representative of the input data. We repeated the sampling process with a specified number of latent vectors from the prior distribution with the learned latent space. This yielded a synthetic dataset with a customized number of samples that represent the experimental data. An example of a generated posterior distribution in relation to the real data is shown in Figure 3.4. Figure 3.4 also indicates that the data was normalized using Z-score normalization with a standard deviation of one. This was used to standardize the ECM parameters and output as some features have different magnitudes.

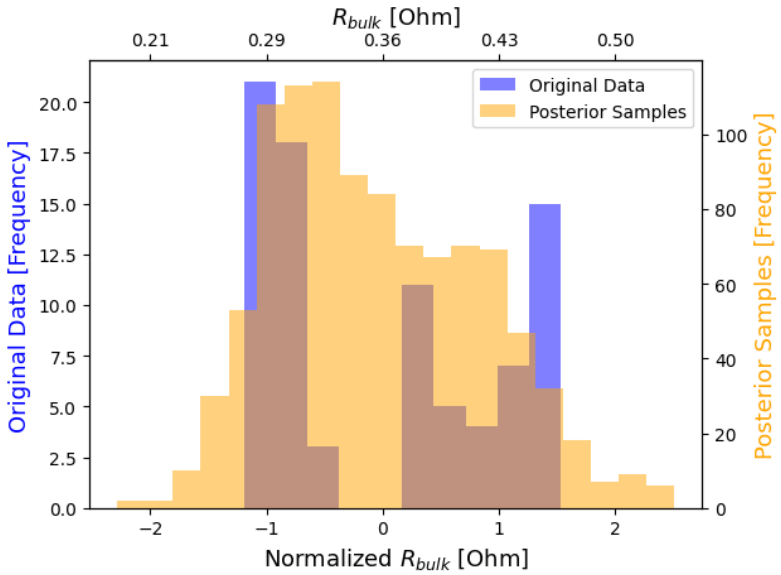

Figure 3.4: Histogram of prior and posterior data distributions overlaid for bulk resistance.

Figure 3.4 shows that the learned posterior normal distribution mimics the experimental data well and removes sparsity from the dataset. When implementing this method, it is important to ensure adequate diversity in the dataset as the VAE will not extrapolate far outside of the original dataset's domain. VAE training and histograms of additional features can be found in Appendix A.2.3.

Important VAE hyper-parameters include the number of input features, the dimensions of the latent space, and the number of samples drawn. The input feature vector includes the ECM parameters, R_{bulk}, R_{sei}, R_{ct}, R_w, CPE_1, CPE_2, and the RUL. Although the RUL is our output data, it must be augmented with the input data to maintain its correlation. The RUL is removed from the synthetic data vector to be used as the labels for the classifier in training. A diagram of the VAE including important hyperparameters is provided in Figure 3.5.

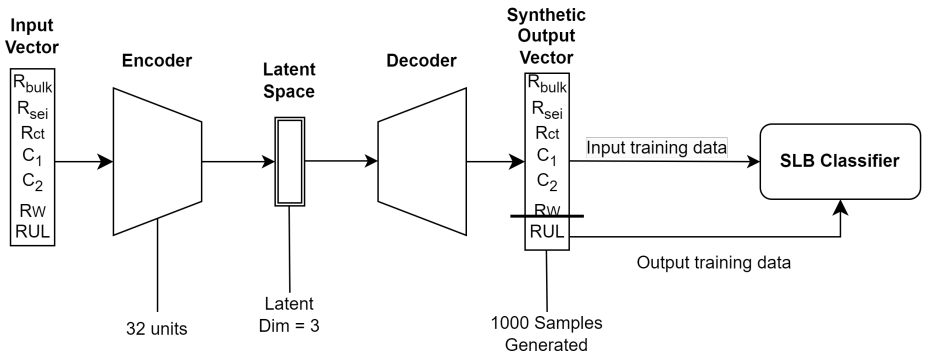

Figure 3.5: Schematic of variational autoencoder data augmentation for classifier training.

Classifier

With the generated synthetic dataset, the binary classification model is trained with the selected input features: R_{bulk}, R_{sei}, R_{ct}, R_w. Binary classification is a common task in machine learning that is used to categorize elements into one of two classes, based on the given input features. Binary classification models are often applied to failure detection problems which aligns with the goals of this project [100]. Classification algorithms such as Logistic Regression, Naive Bayes, K-Nearest Neighbors, and Random Forest were tested to determine the best fit for this data.

An added benefit to these algorithms is their ability to quantify uncertainty. The uncertainty is represented by the model's probability of choosing one output from the other [101]. This gives the model user insight into how close the battery is to being classified in the other grouping.

Once the model is trained it is vital to test on unseen data. For data-driven models in the battery space, the leave-one-out method of cross-validation is useful [102]. A chosen test cell was held out from the VAE data augmentation process. The prediction accuracy is reported by repeating the data generation, model training and testing process with a different test cell 5 times.

3.4 Results

This section compares different machine-learning model test results for this task to determine the strongest algorithm. We compare these results to SOH-based sorting

and ensure our results by repeating the same process with another dataset meeting objectives three and four. The model prediction uncertainty is analyzed along with a regression model for direct degradation rate prediction. Finally, we analyze retired EV module pilot EIS data.

3.4.1 Model Comparison

To label the SLBs as either ready for repurposing or recycling a boundary must be defined to split these two categories. We outline five scenarios representing real-world decisions to test the model's performance sensitivity under different RUL boundaries, including splitting by user-defined thresholds and quantile splits.

User-defined thresholds reflect that the threshold degradation rate may change based on the users preferences. For example, SLBs to be used in vehicles may require a higher tolerance as compared to batteries fit for a backup system. A threshold could also eliminate batteries that fail a degradation warranty or break-even point. The user-defined thresholds tested in this analysis include 5% and 10% SOH loss per 100 cycles.

In addition to the user-defined threshold, quantile splits allow the model user to sort the batteries based on their stock; for example, if a battery is within the top 25% of an inventory. The quantile-split cases tested in this analysis split the data recycle/reuse with ratios of 50/50, 75/25, and 25/75. Table 3.1 shows each tested model's performance accuracy over the discussed use cases.

Table 3.1: Comparing test results from different machine learning models based on percentage accuracy.

	Stock Split			**% loss in 100 cycles**	
Model	**50/50**	**75/25**	**25/75**	**5%**	**10%**
Logistic Regression	92.3%	98.1%	92.3%	85.6%	92.3%
LR (No VAE)	94.5%	82.4%	92.9%	63.6%	90.8%
K-Nearest Neighbours	94.2%	98.0%	92.3%	89.4%	92.3%
Random Forest	82.7%	86.5%	93.2%	86.5%	87.5%
Naive Bayes	84.6%	99.0%	92.3%	67.3%	87.5%

As outlined in Table 3.1, both the logistic regression and K-Nearest Neighbours algorithms are well suited to this task with good accuracy and consistency. The

logistic regression is preferred in this application due to the stronger probability estimation capabilities. This algorithm had an average accuracy of $91.8 \pm 4.4\%$ across the five scenarios. The same cases were tested without the use of the VAE for dataset augmentation and yielded an average of $84.9 \pm 12.8\%$ accuracy. Comparing cases, the VAE data augmentation adds consistency to the result accuracy. This shows the benefit of using a VAE, as sampling from the posterior distribution helps to fill in the gaps in sparse datasets.

3.4.2 Independent Dataset

Our independent dataset was tested by splitting and executing a 90-10 training-testing split 60 times using k-fold validation. For this scenario, we performed a 50/50 class split and achieved 90% accuracy, which aligns with the results using the Zhang dataset. In this case, logistic regression was also the strongest model. The results are displayed using a confusion matrix in Figure 3.6.

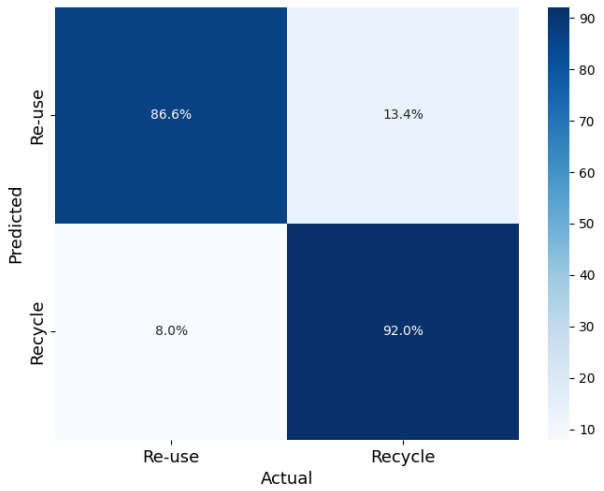

Figure 3.6: Confusion matrix visualization of secondary dataset predictions.

3.4.3 Uncertainty

Quantification of the uncertainty in a data-driven model's prediction adds practicality and confidence in the SLB classification. The logistic regression model is designed specifically for binary classification tasks, as it uses a sigmoid function. Logistic regression divides a dataset by mapping a weighted linear combination of the input features between 0 and 1. Any value above 0.5 is considered useful for second life, and

those below are to be recycled [103, 104]. The predicted value is interpreted as the probability of the prediction, with 1 being 100% probability of being used for second life. Caution is advised for any predictions that are within the 5-95% probability range, as these batteries fall close to the class boundary. Figure 3.7 shows the test results for each cell using the one-in-on-out method on the 25/75 split.

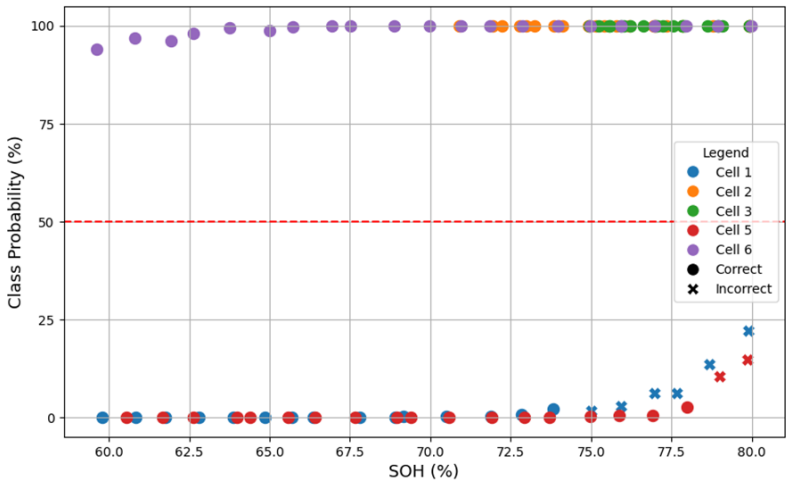

Figure 3.7: Class probability of all test cells in relation to SOH using ECM input feature for the 25/75 test case.

Based on the probability plot, we can see that the model's only mistakes are made at the beginning of Cell 1 and 5's life. The probability estimates of these cases showed that these predictions should be further investigated as the model was not fully confident. Figure 3.7 shows that the model can accurately decipher the rapidly decaying cells from the healthier cells regardless of their SOH with confidence.

These results were compared to how the model performs using SOH as the input. Over the five tested scenarios, this method had an accuracy of 72.9%. As expected, based on the outlined class boundary, the model would draw a line at a certain SOH value. While the lack of capacity is ultimately the reason the battery is retired from first life, it cannot be trusted as an indication of the battery's future health. This is visualized in Figure 3.8 in a 25/75 split. The results for each of the tested cases can be found in Appendix A.2.5.

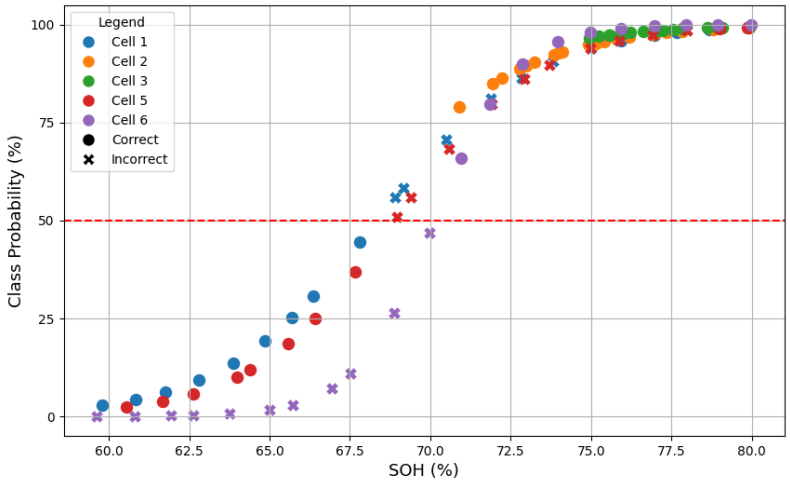

Figure 3.8: Class probability of all test cells in relation to SOH using SOH as the input feature for the 25/75 test case.

3.4.4 Regression

We implement a regression model to test the model's accuracy when forecasting the rate of capacity fade. In this study, we focused on classifying with a pass/fail strategy, but we analyzed the results of this regression to gain further insight into the model's performance.

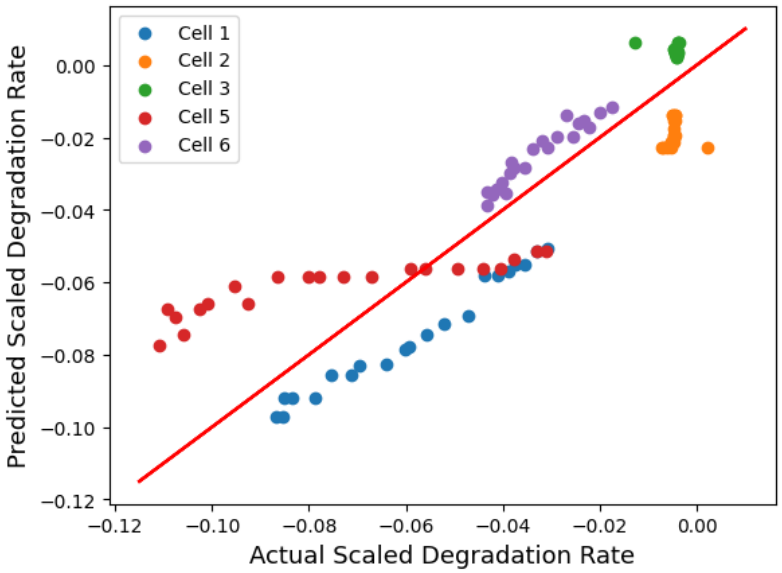

Figure 3.9: Results for direct RUL estimation using a KNN regression.

As shown in Figure 3.9, the K-Nearest Neighbours model struggled to make precise predictions but did follow the right trend yielding an R-squared value of 0.82. It is inferred that some accuracy is lost in the synthetic data sampling process. Consideration of this trade-off implies that synthetic data from VAEs may aid in classification tasks, but larger datasets of real data should be used for regression problems.

3.4.5 Module Test

We have conducted a test using Nissan Leaf modules to address the feasibility of using EIS for SLB sorting. In the preliminary stages of a recent cycle testing experiment on SLBs we performed characterization tests using EIS. This pilot study determines if any modules are not suitable for second-life applications. Upon receiving the modules, EIS is applied to each one and visualized in the Nyquist plots in Figure 3.10.

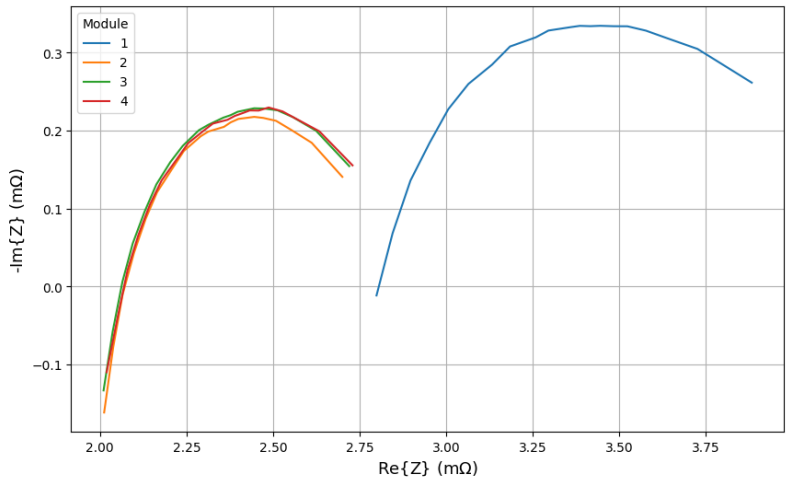

Figure 3.10: Nyqusit plot of characterization impedance measurements on Nissan Leaf modules.

The Nyquist plots suggest that Module 1 has a significantly higher impedance than the other modules and therefore is not viable for second life. As we are restricted to cell-level cycling equipment to verify our decision-making we checked the capacity of each cell. The cell capacities are tabulated in Table 3.2. Cell 12 is missing as one of the cell terminal tabs was damaged during the module deconstruction.

Table 3.2: Module data including capacities and voltages.

Module #	Module 1	Module 2	Module 3	Module 4
Voltage (V)	7.24	7.43	7.15	7.18
Cell 1 Capacity (Ah)	19.82	23.61	24.31	24.12
Cell 2 Capacity (Ah)	19.75	24.02	24.09	23.09
Cell 3 Capacity (Ah)	18.97	23.61	24.37	23.57
Cell 4 Capacity (Ah)	19.44	22.92	—	24.27
Module Capacity (Ah)	38.41	46.53	48.40	47.21

By summing the capacity of cells in parallel and taking the minimum of those in series, module capacity is calculated and tabulated in Table 3.2. These measurements are taken at unknown SOC, and the voltages are reported through multimeter readings. Module 1 has significantly less capacity in comparison to its counterparts. As all of these modules were drawn from the same pack, it is assumed they experienced the same cycling conditions, except for varying temperature gradients. This indicates module 1 has been experiencing accelerated degradation. This shows promise for using EIS to sort SLBs on parallel/series-connected cell groups.

3.5 Discussion

In the previous section, we demonstrated the results and validation of our methodology. Our discussion will centre upon the significance, key takeaways, and limitations of our model results, methodology, and data augmentation.

3.5.1 Results Evaluation

This study aimed to decipher between batteries for second-life applications or recycling with minimal characterization testing. This was achieved using EIS measurements that inform a binary classification model fitted with probability prediction. The reason for testing this method on second-life battery data is to highlight the volatility of degradation as time goes on, requiring information beyond the battery's capacity. Out of the four classification models tested the logistic regression yielded the strongest results with an average accuracy of 91.8% across all test scenarios. The logistic regression algorithm also performed best on our secondary dataset with an accuracy of 90%. This performance aligns with existing classification models for remaining useful life as

they have reported accuracies between 88 and 97% [76, 79, 105]. EIS outperformed a capacity informed model by 20% accuracy. This allows us to showcase that drawing a line strictly based on capacity will result in inaccurate sorting. While reading an EVs battery range is a quick way to sort EIS offers increased accuracy at negligible time costs. After user assessment battery packs must undergo a UL-certified inspection and grading procedure before they can be used in second-life applications [106]. Our method will weed out packs that are not worthy of the time and money required to complete this certification, aiding in the profitability of the SLB industry. This will also eliminate packs vulnerable to thermal runaway due to high internal resistance that may fail certification.

3.5.2 Model Application

When considering the barriers to implementing SLB sorting methods in the real world we must account for the time and economic investment. In a scenario where a battery repurposing company is grading multiple batteries every day the difference in testing times between weeks, days, hours and minutes is significant. Unlike methods that require multiple cycles to make a prediction, our method requires no cycling and only minutes to complete testing. EIS also has the flexibility to be performed on the pack level which is the most practical due to the cost of battery pack disassembly. We performed a trial experiment to test the abilities of EIS for SLB selection on series/parallel connected cells. The analysis showed promise as the Nyquist plots show a clear outlier, revealing the weakest battery module. The EIS testing took minutes to complete and was noninvasive displaying its practicality.

When testing our proposed algorithm, we outlined five different scenarios where the model user would adjust the threshold of what makes a good battery. These cases are determined by either setting the threshold based on a defined rate of degradation or splitting the data based on quantiles. Splitting by a RUL threshold is useful when the SLB use case has a specific safety factor or degradation rate you do not want to surpass. Splitting by quantile assesses the battery in comparison to the training set and categorizes whether it is above or below your defined percentile. This could be useful for identifying outliers or segmenting the best stock. The accuracy for each of the test cases was strong and found that most of the mistakes were at the boundary between the two classes. The probability estimate allows the model user to make a judgement call when closer to the borderline.

A limitation of EIS is its sensitivity to battery SOC and temperature. The data used in this study was collected at a consistent temperature and full SOC. Without proper implementation, EIS measurements at different SOCs and temperatures could affect model accuracy. We also assume that ECM parameters would have the same trends with batteries of different chemistries. Physically, as the capacity declines and degradation mechanisms propagate ECM resistances will increase, however, the dominant parameters may vary between chemistries. This was observed in our second dataset as the CPE1 parameter had stronger correlations with RUL than Rsei, so it was swapped in its place.

3.5.3 Data Augmentation

This study also addresses the lack of publicly available data for SLB degradation. While models have explored the volatility of SLBs they are limited in the ability to train data-driven models for RUL prediction on real-world representative data [69, 70, 72]. Commonly, RUL predictions that account for the knee point are subject to accelerated degradation testing conditions, which yield predictable capacity fade trajectories, removing some of the uncertainty of second life [76, 77]. This early onset knee point may be a result of inadequate SEI formation. To bridge the gap between small more variable and larger accelerated datasets we used a VAE to learn a representative distribution of the experimental data. This distribution can be repeatedly sampled producing a method of applying smaller experimental datasets to data-driven models. The model is compared with and without adding the VAE, resulting in a 6.9% discrepancy in prediction accuracy. Quantifying the importance of this accuracy boost goes beyond classifying 7 more batteries correctly out of 100. The VAE added consistency across the test cases with an 8.4% difference in standard deviation. As machine learning models often face backlash for mistakes, added consistency fosters trust in the model.

3.5.4 Future Work

Future work may include acquiring EIS at different SOCs and temperatures that mimic more realistic conditions. It would be particularly interesting to test this method using EIS data taken from EV batteries at the pack level that have been left at rest for long periods, as this parallels the current state of the market. In this case, a voltage feature should be added to the model inputs as an indication of SOC. To

further explore the applicability of this model an in-depth techno-economic analysis should be conducted. This may include costs of EIS equipment, SLB profitability based on application, and financial risk of premature failure. EIS hardware can be prohibitively expensive, comparing this to cyclers and factoring in testing time may provide a better understanding of method feasibility. Deeper analysis of the Zhang dataset could consist of a more extensive sensitivity analysis of the classification threshold, to ensure good model accuracy for any possible case. With access to a larger dataset or with the use of transfer learning it is recommended that direct RUL prediction for SLBs using EIS is further investigated.

Chapter 4

Conclusions

4.1 Conclusions

Lithium-ion battery degradation is variable and requires monitoring for adequate lifespan and safety. The objective of this work was to develop methods for quickly gaining deeper insights into battery degradation using data-driven modelling. We chose tasks that reflect battery usage in the first and second life, using real-time and future predictions connected by using EIS data. EIS is a focus of this work due to its prowess as a fast in-situ measurement, with insights into internal battery degradation.

Starting with first life, we quantified degradation modes using EIS data and equivalent circuit modelling. As the battery degrades, we see the non-uniformity in degradation mode propagation, leading us to believe that this information can indicate future degradation. We implemented a Random Forest machine learning algorithm to predict these degradation modes in real time using feature-engineered charging data. We captured 95, 98, and 91% of degradation mode variance over cell cycle life when predicting the conductivity loss, loss of lithium inventory, and loss of active material, respectively. Discrepancies in prediction accuracy could be attributed to the correlations between model input charging features and target DMs. The accuracy of individual DM prediction was improved by focusing on specific areas of the CC or CV curves that show higher Shapley feature importance. This provides a method of rapidly characterizing battery health on a deeper level without needing onboard EIS hardware.

After a battery is retired from its first life application, a decision regarding whether it should be reused or recycled must be made. Second-life batteries are volatile and arrive at varied SOHs, warranting a health screening method before use. We can leverage the same EIS quantified degradation modes as model inputs, this time to determine future battery viability. A logistic regression classification algorithm filters out future failing batteries with a single EIS measurement, saving battery repurposers time and money. Using a sensitivity analysis to adjust the class boundary, we find that the model remains consistent with an average accuracy of 92%.

These two methods provide frameworks for determining key health metrics that aid financial, safety, and operational-based decision-making. This work highlights the importance of gaining deeper insights into battery degradation due to variance, particularly observed in the later stages of life. Machine learning is applied as it is a quickly parameterized modelling technique that can decipher complex relationships in large datasets. As rigorous data acquisition becomes a standard in battery ESS and EVs, machine learning can take advantage of this to quantify useful health metrics with appropriate data processing and problem definition. To add model interpretability visualizations were used to display input feature importance in DM quantification, and uncertainty in our classification predictions. Using machine learning algorithms, we are conscious of the practical accessibility of the input data relative to the importance of the given task. EIS proves to be a useful tool for quantifying complex LIB degradation and will continue to grow in real-world applications as hardware improvements are made.

4.2 Future Work

A common source of future work in battery degradation modelling is model validation on different datasets. For our work in Chapter 2, testing our methodology on LIBs of different cathode chemistry and a wider array of degradation pathways would be useful. This dataset focussed primarily on the variance in degradation due to depth of discharge. Cycling at varying temperatures and higher C-rates could result in more extensive pathways, further inducing conductivity loss. Implementing the use of synthetic data, transfer learning, or pre-trained time-series models are methods that could allow for more complex pattern recognition within the charging curves. The shapely analysis could also be consulted to choose charging segments to focus on

in further testing.

In Chapter 3, similar points regarding data variety may be made. The method was tested on another dataset achieving similar results, proving model consistency over differing chemistries and degradation pathways. An interesting source of focus of future work for this study may include an in-depth techno-economic analysis. To justify the use of EIS, the costs of equipment and testing time may be compared to more common cycling-based characterization methods. An economic sensitivity analysis could also be conducted to determine optimal boundary thresholds for separating second-life-worthy batteries from those that are not. This would entail using degradation rates and initial capacities at the point of first-life retirement to see how these factors affect project profitability.

Generally, further work can be done to eliminate the need for lab conditions which is a greater issue in the battery modelling space. This would include sizing up to the module or pack level, as labs are commonly restricted to testing on cells. We are in the process of producing a second-life battery dataset equipped with continuous EIS and temperature variation to capture measurement deviation due to temperature, SOC, and degradation in second-life batteries. This would offer further data to test our sorting method and provide more second-life battery data to a data-scarce field. The final frontier of this thesis would be extracting constant current and voltage charging data from an EV's BMS in operation to determine degradation modes in real time. When this vehicle retires, a decision regarding second-life viability can be made using these predictions as inputs for our classification algorithm. This model-chaining approach effectively incorporates decision-making across the entire lifespan of the battery.

Bibliography

[1] Battery recycling takes the drivers seat | McKinsey. https://www.mckinsey.com/industries/automotive-and-assembly/our-insights/battery-recycling-takes-the-drivers-seat, 2023.

[2] Yi Li, Kailong Liu, Aoife M. Foley, Alana Zlke, Maitane Berecibar, Elise Nanini-Maury, Joeri Van Mierlo, and Harry E. Hoster. Data-driven health estimation and lifetime prediction of lithium-ion batteries: A review. *Renewable and Sustainable Energy Reviews*, 113:109254, 2019.

[3] Yifei Zhou, Shunli Wang, Yanxing Xie, Xianfeng Shen, and Carlos Fernandez. Remaining useful life prediction and state of health diagnosis for lithium-ion batteries based on improved grey wolf optimization algorithm-deep extreme learning machine algorithm. *Energy*, 285:128761, 2023.

[4] Yunwei Zhang, Qiaochu Tang, Yao Zhang, Jiabin Wang, Ulrich Stimming, and Alpha A. Lee. Identifying degradation patterns of lithium ion batteries from impedance spectroscopy using machine learning. *Nature Communications*, 11:1706, 2020.

[5] Transport Canada. Canada's zero-emission vehicle sales targets, 2024. https://tc.canada.ca/en/road-transportation/innovative-technologies/zero-emission-vehicles/canada-s-zero-emission-vehicle-sales-targets, 2024.

[6] Transport Canada. Transport canada greenhouse gas emissions, 2022. https://tc.canada.ca/en/corporate-services/transparency/corporate-management-reporting/transportation-canada-annual-reports/2021/greenhouse-gas-emissions, 2022.

[7] Canada - countries & regions. https://www.iea.org/countries/canada, 2024.

[8] Margaret Slattery, Jessica Dunn, and Alissa Kendall. Charting the electric vehicle battery reuse and recycling network in north america. *Waste Management*, 174:76–87, 2024.

[9] Qingyin Dong, Shuang Liang, Jinhui Li, Hyung Chul Kim, Wei Shen, and Timothy J. Wallington. Cost, energy, and carbon footprint benefits of second-life electric vehicle battery use. *iScience*, 26(7):107195, 2023.

[10] Dipti Kamath, Renata Arsenault, Hyung Chul Kim, and Annick Anctil. Economic and environmental feasibility of second-life lithium-ion batteries as fast-charging energy storage. *Environmental Science & Technology*, 54(11):6878–6887, 2020. Publisher: American Chemical Society.

[11] Dipti Kamath, Siddharth Shukla, Renata Arsenault, Hyung Chul Kim, and Annick Anctil. Evaluating the cost and carbon footprint of second-life electric vehicle batteries in residential and utility-level applications. *Waste Management*, 113:497–507, 2020.

[12] Kirti Richa, Callie W. Babbitt, Nenad G. Nenadic, and Gabrielle Gaustad. Environmental trade-offs across cascading lithium-ion battery life cycles. *The International Journal of Life Cycle Assessment*, 22(1):66–81, 2017.

[13] K. E. D. Global. Battery recycling: Carmakers, battery companies in new turf war. https://www.kedglobal.com/battery-recycling/newsView/ked202108160002, 2021.

[14] Carlos Henrique Illa Font, Hugo Valadares Siqueira, Joo Eustquio Machado Neto, Joo Lucas Ferreira dos Santos, Sergio Luiz Stevan, Attilio Converti, and Fernanda Cristina Corra. Second life of lithium-ion batteries of electric vehicles: A short review and perspectives. *Energies*, 16(2):953, 2023. Number: 2 Publisher: Multidisciplinary Digital Publishing Institute.

[15] Peter M. Attia, Alexander Bills, Ferran Brosa Planella, Philipp Dechent, Gonalo dos Reis, Matthieu Dubarry, Paul Gasper, Richard Gilchrist, Samuel Greenbank, David Howey, Ouyang Liu, Edwin Khoo, Yuliya Preger, Abhishek Soni, Shashank Sripad, Anna G. Stefanopoulou, and Valentin Sulzer. Reviewknees in lithium-ion battery aging trajectories. *Journal of The Electrochemical Society*, 169(6):060517, 2022. Publisher: IOP Publishing.

[16] Yang Gao, Jiuchun Jiang, Caiping Zhang, Weige Zhang, Zeyu Ma, and Yan Jiang. Lithium-ion battery aging mechanisms and life model under different charging stresses. *Journal of Power Sources*, 356:103–114, 2017-07-15.

[17] M. M. Kabir and Dervis Emre Demirocak. Degradation mechanisms in li-ion batteries: a state-of-the-art review. *International Journal of Energy Research*, 41(14):1963–1986, 2017. _eprint: https://onlinelibrary.wiley.com/doi/pdf/10.1002/er.3762.

[18] Xianke Lin, Kavian Khosravinia, Xiaosong Hu, Ju Li, and Wei Lu. Lithium plating mechanism, detection, and mitigation in lithium-ion batteries. *Progress in Energy and Combustion Science*, 87:100953, 2021-11-01.

[19] Dongqing Liu, Zulipiya Shadike, Ruoqian Lin, Kun Qian, Hai Li, Kaikai Li, Shuwei Wang, Qipeng Yu, Ming Liu, Swapna Ganapathy, Xianying Qin, Quan-Hong Yang, Marnix Wagemaker, Feiyu Kang, Xiao-Qing Yang, and Baohua Li. Review of recent development of in situ/operando characterization techniques for lithium battery research. *Advanced Materials*, 31(28):1806620, 2019. _eprint: https://onlinelibrary.wiley.com/doi/pdf/10.1002/adma.201806620.

[20] Woosung Choi, Heon-Cheol Shin, Ji Man Kim, Jae-Young Choi, and Won-Sub Yoon. Modeling and applications of electrochemical impedance spectroscopy (EIS) for lithium-ion batteries. *Journal of Electrochemical Science and Technology*, 11(1):1–13, 2020.

[21] Li-fan Wang, Meng-meng Geng, Xia-nan Ding, Chen Fang, Yu Zhang, Shanshan Shi, Yong Zheng, Kai Yang, Chun Zhan, and Xin-dong Wang. Research progress of the electrochemical impedance technique applied to the high-capacity lithium-ion battery. *International Journal of Minerals, Metallurgy and Materials*, 28(4):538–552, 2021-04-01.

[22] Miquel Mart-Florences, Andreu Cecilia, and Ramon Costa-Castell. Modelling and estimation in lithium-ion batteries: A literature review. *Energies*, 16(19):6846, 2023. Number: 19 Publisher: Multidisciplinary Digital Publishing Institute.

[23] S. Tamilselvi, S. Gunasundari, N. Karuppiah, Abdul Razak RK, S. Madhusudan, Vikas Madhav Nagarajan, T. Sathish, Mohammed Zubair M. Shamim,

C. Ahamed Saleel, and Asif Afzal. A review on battery modelling techniques. *Sustainability*, 13(18):10042, 2021. Number: 18 Publisher: Multidisciplinary Digital Publishing Institute.

[24] Gonalo dos Reis, Calum Strange, Mohit Yadav, and Shawn Li. Lithium-ion battery data and where to find it. *Energy and AI*, 5:100081, 2021-09-01.

[25] Reza Rouhi Ardeshiri, Bharat Balagopal, Amro Alsabbagh, Chengbin Ma, and Mo-Yuen Chow. Machine learning approaches in battery management systems: State of the art: Remaining useful life and fault detection. In *2020 2nd IEEE International Conference on Industrial Electronics for Sustainable Energy Systems (IESES)*, volume 1, pages 61–66, 2020.

[26] Vankamamidi S. Naresh, Guduru V. N. S. R. Ratnakara Rao, and D. V. N. Prabhakar. Predictive machine learning in optimizing the performance of electric vehicle batteries: Techniques, challenges, and solutions. *WIREs Data Mining and Knowledge Discovery*, 14(5):e1539, 2024. _eprint: https://onlinelibrary.wiley.com/doi/pdf/10.1002/widm.1539.

[27] Zahra Nozarijouybari and Hosam K. Fathy. Machine learning for battery systems applications: Progress, challenges, and opportunities. *Journal of Power Sources*, 601:234272, 2024-05-01.

[28] Carlos Pastor-Fernndez, W. Dhammika Widanage, James Marco, Miguel-ngel Gama-Valdez, and Gael. H. Chouchelamane. Identification and quantification of ageing mechanisms in lithium-ion batteries using the EIS technique. In *2016 IEEE Transportation Electrification Conference and Expo (ITEC)*, pages 1–6, 2016.

[29] Carlos Pastor-Fernndez, Tung Fai Yu, W. Dhammika Widanage, and James Marco. Critical review of non-invasive diagnosis techniques for quantification of degradation modes in lithium-ion batteries. *Renewable and Sustainable Energy Reviews*, 109:138–159, 2019.

[30] Ruilong Xu, Yujie Wang, and Zonghai Chen. Data-driven battery aging mechanism analysis and degradation pathway prediction. *Batteries*, 9(2):129, 2023. Number: 2 Publisher: Multidisciplinary Digital Publishing Institute.

[31] Matthieu Dubarry, Cyril Truchot, and Bor Yann Liaw. Cell degradation in commercial LiFePO4 cells with high-power and high-energy designs. *Journal of Power Sources*, 258:408–419, 2014.

[32] Meinert Lewerenz, Andrea Marongiu, Alexander Warnecke, and Dirk Uwe Sauer. Differential voltage analysis as a tool for analyzing inhomogeneous aging: A case study for LiFePO4|graphite cylindrical cells. *Journal of Power Sources*, 368:57–67, 2017.

[33] A. Fly and R. Chen. Rate dependency of incremental capacity analysis (dQ/dV) as a diagnostic tool for lithium-ion batteries. *Journal of Energy Storage*, 29:101329, 2020.

[34] Kamala Kumari Duru, Praneash Venkatachalam, Chanakya Karra, Asha Anish Madhavan, Sangaraju Sambasivam, and Sujith Kalluri. Equivalent circuit model parameters estimation of lithium-ion batteries using cuckoo search algorithm. *Journal of The Electrochemical Society*, 169(12):120503, 2022. Publisher: IOP Publishing.

[35] Carlos Pastor-Fernndez, Kotub Uddin, Gael H. Chouchelamane, W. Dhammika Widanage, and James Marco. A comparison between electrochemical impedance spectroscopy and incremental capacity-differential voltage as li-ion diagnostic techniques to identify and quantify the effects of degradation modes within battery management systems. *Journal of Power Sources*, 360:301–318, 2017.

[36] Hao Sun, Bo Jiang, Heze You, Bojian Yang, Xueyuan Wang, Xuezhe Wei, and Haifeng Dai. Quantitative analysis of degradation modes of lithium-ion battery under different operating conditions. *Energies*, 14(2):350, 2021. Number: 2 Publisher: Multidisciplinary Digital Publishing Institute.

[37] Xing Shu, Shiquan Shen, Jiangwei Shen, Yuanjian Zhang, Guang Li, Zheng Chen, and Yonggang Liu. State of health prediction of lithium-ion batteries based on machine learning: Advances and perspectives. *iScience*, 24(11):103265, 2021.

[38] Chuanping Lin, Jun Xu, Mingjie Shi, and Xuesong Mei. Constant current charging time based fast state-of-health estimation for lithium-ion batteries. *Energy*, 247:123556, 2022.

[39] Haijun Ruan, Jingyi Chen, Weilong Ai, and Billy Wu. Generalised diagnostic framework for rapid battery degradation quantification with deep learning. *Energy and AI*, 9:100158, 2022.

[40] Weihan Li, Jue Chen, Katharina Quade, Daniel Luder, Jingyu Gong, and Dirk Uwe Sauer. Battery degradation diagnosis with field data, impedance-based modeling and artificial intelligence. *Energy Storage Materials*, 53:391–403, 2022.

[41] Giovanna Oriti, Alexander L. Julian, and Peter Norgaard. Battery management system with cell equalizer for multi-cell battery packs. In *2014 IEEE Energy Conversion Congress and Exposition (ECCE)*, pages 900–905, 2014. ISSN: 2329-3748.

[42] *Product data sheet, INR-21700-P42A, Molicel*, 2023-09.

[43] Ankit Bhatt, Weerakorn Ongsakul, Nimal Madhu Manjiparambil, and Jai Govind Singh. Machine learning-based approach for useful capacity prediction of second-life batteries employing appropriate input selection. *International Journal of Energy Research*, 45(15):21023–21049, 2021. _eprint: https://onlinelibrary.wiley.com/doi/pdf/10.1002/er.7160.

[44] Yongquan Sun, Xueling Hao, Michael Pecht, and Yapeng Zhou. Remaining useful life prediction for lithium-ion batteries based on an integrated health indicator. *Microelectronics Reliability*, 88-90:1189–1194, 2018.

[45] Matthew D. Murbach, Brian Gerwe, Neal Dawson-Elli, and Lok kun Tsui. impedance.py: A python package for electrochemical impedance analysis. *Journal of Open Source Software*, 5(52):2349, 2020.

[46] Circuit lab, https://www.circuitlab.com, 2023.

[47] Sadia Tasnim Mowri, Anup Barai, Aniruddha Gupta, and James Marco. Verification of the modified degradation mode identification technique by employing electrochemical impedance spectroscopy and differential voltage analysis. *Batteries*, 8(12):274, 2022. Number: 12 Publisher: Multidisciplinary Digital Publishing Institute.

[48] Fabian Pedregosa, Gal Varoquaux, Alexandre Gramfort, Vincent Michel, Bertrand Thirion, Olivier Grisel, Mathieu Blondel, Peter Prettenhofer, Ron Weiss, Vincent Dubourg, Jake Vanderplas, Alexandre Passos, David Cournapeau, Matthieu Brucher, Matthieu Perrot, and douard Duchesnay. Scikit-learn: Machine learning in python. *Journal of Machine Learning Research*, 12(85):2825–2830, 2011.

[49] Andreas C. Mller and Sarah Guido. *Introduction to Machine Learning with Python: A Guide for Data Scientists*. "O'Reilly Media, Inc.", 2016.

[50] Xinyu Jia, Caiping Zhang, Linjing Zhang, Weige Zhang, and Zhongling Xu. Identification method and quantification analysis of the critical aging speed interval for battery knee points. *World Electric Vehicle Journal*, 14(12):346, 2023. Number: 12 Publisher: Multidisciplinary Digital Publishing Institute.

[51] Iman Babaeiyazdi, Afshin Rezaei-Zare, and Shahab Shokrzadeh. Transfer learning with deep neural network for capacity prediction of li-ion batteries using EIS measurement. *IEEE Transactions on Transportation Electrification*, pages 1–1, 2022. Conference Name: IEEE Transactions on Transportation Electrification.

[52] Tadayoshi Fushiki. Estimation of prediction error by using k-fold cross-validation. *Statistics and Computing*, 21(2):137–146, 2011.

[53] Sergiu Hart. Shapley value. In John Eatwell, Murray Milgate, and Peter Newman, editors, *Game Theory*, The New Palgrave, pages 210–216. Palgrave Macmillan UK, 1989.

[54] Mona Faraji Niri, Koorosh Aslansefat, Sajedeh Haghi, Mojgan Hashemian, Rdiger Daub, and James Marco. A review of the applications of explainable machine learning for lithiumion batteries: From production to state and performance estimation. *Energies*, 16(17):6360, 2023. Number: 17 Publisher: Multidisciplinary Digital Publishing Institute.

[55] Scott M. Lundberg, Gabriel Erion, Hugh Chen, Alex DeGrave, Jordan M. Prutkin, Bala Nair, Ronit Katz, Jonathan Himmelfarb, Nisha Bansal, and Su-In Lee. From local explanations to global understanding with explainable AI for trees. *Nature Machine Intelligence*, 2(1):56–67, 2020. Number: 1 Publisher: Nature Publishing Group.

[56] Hanna Meyer and Edzer Pebesma. Predicting into unknown space? estimating the area of applicability of spatial prediction models. *Methods in Ecology and Evolution*, 12(9):1620–1633, 2021. _eprint: https://onlinelibrary.wiley.com/doi/pdf/10.1111/2041-210X.13650.

[57] Fatemeh Hateffard, Luc Steinbuch, and Gerard B. M. Heuvelink. Evaluating the extrapolation potential of random forest digital soil mapping. *Geoderma*, 441:116740, 2024.

[58] Bo Pang, Li Chen, and Zuomin Dong. Data-driven degradation modeling and SOH prediction of li-ion batteries. *Energies*, 15(15):5580, 2022. Number: 15 Publisher: Multidisciplinary Digital Publishing Institute.

[59] Yunjian Li, Kuining Li, Yi Xie, Jiangyan Liu, Chunyun Fu, and Bin Liu. Optimized charging of lithium-ion battery for electric vehicles: Adaptive multi-stage constant currentconstant voltage charging strategy. *Renewable Energy*, 146:2688–2699, 2020.

[60] Pengju Cao, Yunyu Tang, Fan Zhu, Zhuhaobo Zhang, Jing Zhou, Zhihong Bai, and Hao Ma. An IPT system with constant current and constant voltage output features for EV charging. In *IECON 2018 - 44th Annual Conference of the IEEE Industrial Electronics Society*, pages 4775–4780, 2018. ISSN: 2577-1647.

[61] C. H. Dharmakeerthi, N. Mithulananthan, and T. K. Saha. Impact of electric vehicle fast charging on power system voltage stability. *International Journal of Electrical Power & Energy Systems*, 57:241–249, 2014.

[62] Manh-Kien Tran, Andre DaCosta, Anosh Mevawalla, Satyam Panchal, and Michael Fowler. Comparative study of equivalent circuit models performance in four common lithium-ion batteries: LFP, NMC, LMO, NCA. *Batteries*, 7(3):51, 2021. Number: 3 Publisher: Multidisciplinary Digital Publishing Institute.

[63] Mohamed Ahmeid, Musbahu Muhammad, Simon Lambert, Pierrot S. Attidekou, and Zoran Milojevic. A rapid capacity evaluation of retired electric vehicle battery modules using partial discharge test. *Journal of Energy Storage*, 50:104562, 2022.

[64] Lithium-ion battery demand forecast for 2030 | McKinsey. https://www.mckinsey.com/industries/automotive-and-assembly/our-insights/battery-2030-resilient-sustainable-and-circular, 2024.

[65] B2u storage solutions. https://www.b2uco.com, 2024.

[66] Moment energy - clean, affordable & reliable battery energy storage system. https://www.momentenergy.com/, 2024.

[67] Lluc Canals Casals, B. Amante Garca, and Camille Canal. Second life batteries lifespan: Rest of useful life and environmental analysis. *Journal of Environmental Management*, 232:354–363, 2019.

[68] Toms Montes, Maite Etxandi-Santolaya, Josh Eichman, Victor Jos Ferreira, Llus Trilla, and Cristina Corchero. Procedure for assessing the suitability of battery second life applications after EV first life. *Batteries*, 8(9):122, 2022. Number: 9 Publisher: Multidisciplinary Digital Publishing Institute.

[69] Elisa Braco, Idoia San Martn, Alberto Berrueta, Pablo Sanchis, and Alfredo Ursa. Experimental assessment of cycling ageing of lithium-ion second-life batteries from electric vehicles. *Journal of Energy Storage*, 32:101695, 2020.

[70] E. Coron, S. Genis, M. Cugnet, and P. X. Thivel. Impact of lithium-ion cell condition on its second life viability. *Journal of The Electrochemical Society*, 167(11):110556, 2020. Publisher: IOP Publishing.

[71] Weiping Diao, Jonghoon Kim, Michael H. Azarian, and Michael Pecht. Degradation modes and mechanisms analysis of lithium-ion batteries with knee points. *Electrochimica Acta*, 431:141143, 2022.

[72] Pedro V. H. Seger, Pierre-Xavier Thivel, and Delphine Riu. A second life li-ion battery ageing model with uncertainties: From cell to pack analysis. *Journal of Power Sources*, 541:231663, 2022.

[73] Egoitz Martinez-Laserna, Elixabet Sarasketa-Zabala, Igor Villarreal Sarria, Daniel-Ioan Stroe, Maciej Swierczynski, Alexander Warnecke, Jean-Marc Timmermans, Shovon Goutam, Noshin Omar, and Pedro Rodriguez. Technical viability of battery second life: A study from the ageing perspective. *IEEE Transactions on Industry Applications*, 54(3):2703–2713, 2018. Conference Name: IEEE Transactions on Industry Applications.

[74] Kun Lee and Dongsuk Kum. Development of cell selection framework for second-life cells with homogeneous properties. *International Journal of Electrical Power & Energy Systems*, 105:429–439, 2019.

[75] Selcuk Atalay, Muhammad Sheikh, Alessandro Mariani, Yu Merla, Ed Bower, and W. Dhammika Widanage. Theory of battery ageing in a lithium-ion battery: Capacity fade, nonlinear ageing and lifetime prediction. *Journal of Power Sources*, page 229026, 2020.

[76] Kristen A. Severson, Peter M. Attia, Norman Jin, Nicholas Perkins, Benben Jiang, Zi Yang, Michael H. Chen, Muratahan Aykol, Patrick K. Herring, Dimitrios Fraggedakis, Martin Z. Bazant, Stephen J. Harris, William C. Chueh, and Richard D. Braatz. Data-driven prediction of battery cycle life before capacity degradation. *Nature Energy*, 4(5):383–391, 2019. Publisher: Nature Publishing Group.

[77] Muhammad Haris, Muhammad Noman Hasan, and Shiyin Qin. Degradation curve prediction of lithium-ion batteries based on knee point detection algorithm and convolutional neural network. *IEEE Transactions on Instrumentation and Measurement*, 71:1–10, 2022. Conference Name: IEEE Transactions on Instrumentation and Measurement.

[78] M. Muhammad, M. Ahmeid, P. S. Attidekou, Z. Milojevic, S. Lambert, and P. Das. Assessment of spent EV batteries for second-life application. In *2019 IEEE 4th International Future Energy Electronics Conference (IFEEC)*, pages 1–5, 2019.

[79] Paula Fermn-Cueto, Euan McTurk, Michael Allerhand, Encarni Medina-Lopez, Miguel F. Anjos, Joel Sylvester, and Gonalo dos Reis. Identification and machine learning prediction of knee-point and knee-onset in capacity degradation curves of lithium-ion cells. *Energy and AI*, 1:100006, 2020.

[80] Matthieu Dubarry and David Beck. Big data training data for artificial intelligence-based li-ion diagnosis and prognosis. *Journal of Power Sources*, 479:228806, 2020.

[81] Tobias Hofmann, Jacob Hamar, Bastian Mager, Simon Erhard, and Jan Philipp Schmidt. Transfer learning from synthetic data for open-circuit voltage curve

reconstruction and state of health estimation of lithium-ion batteries from partial charging segments. *Energy and AI*, 17:100382, 2024.

[82] Yan Jiang, Jiuchun Jiang, Caiping Zhang, Weige Zhang, Yang Gao, and Qipei Guo. Recognition of battery aging variations for LiFePO4 batteries in 2nd use applications combining incremental capacity analysis and statistical approaches. *Journal of Power Sources*, 360:180–188, 2017.

[83] Aihua Ran, Zihao Zhou, Shuxiao Chen, Pengbo Nie, Kun Qian, Zhenlong Li, Baohua Li, Hongbin Sun, Feiyu Kang, Xuan Zhang, and Guodan Wei. Data-driven fast clustering of second-life lithium-ion battery: Mechanism and algorithm. *Advanced Theory and Simulations*, 3(8):2000109, 2020. Publisher: John Wiley & Sons, Ltd.

[84] Matthieu Dubarry, Cyril Truchot, and Bor Yann Liaw. Synthesize battery degradation modes via a diagnostic and prognostic model. *Journal of Power Sources*, 219:204–216, 2012.

[85] Yongzhi Zhang, Rui Xiong, Hongwen He, and Michael G. Pecht. Lithium-ion battery remaining useful life prediction with boxcox transformation and monte carlo simulation. *IEEE Transactions on Industrial Electronics*, 66(2):1585–1597, 2019. Conference Name: IEEE Transactions on Industrial Electronics.

[86] Bolun Xu, Alexandre Oudalov, Andreas Ulbig, Gran Andersson, and Daniel S. Kirschen. Modeling of lithium-ion battery degradation for cell life assessment. *IEEE Transactions on Smart Grid*, 9(2):1131–1140, 2018. Conference Name: IEEE Transactions on Smart Grid.

[87] Martin F. Brner, Moritz H. Frieges, Benedikt Spth, Kathrin Sptz, Heiner H. Heimes, Dirk Uwe Sauer, and Weihan Li. Challenges of second-life concepts for retired electric vehicle batteries. *Cell Reports Physical Science*, 3(10):101095, 2022.

[88] Pulsenics. https://www.pulsenics.com/, 2024.

[89] Joseph P. Ross, Efstratios Chatzinikolaou, Damien F. Frost, Stephen R. Duncan, and David A. Howey. Comparison between battery cell level dynamics and pack level dynamics using equivalent circuit models. In *2024 American Control Conference (ACC)*, pages 713–718, 2024. ISSN: 2378-5861.

[90] Wei Gao, Zhi Cao, Naser Vosoughi Kurdkandi, Yuhong Fu, and Chirs Mi. Evaluation of the second-life potential of the first-generation nissan leaf battery packs in energy storage systems. *eTransportation*, 20:100313, 2024.

[91] Paul Gasper, Andrew Schiek, Kandler Smith, Yuta Shimonishi, and Shuhei Yoshida. Predicting battery capacity from impedance at varying temperature and state of charge using machine learning. *Cell Reports Physical Science*, 3(12), 2022. Publisher: Elsevier.

[92] Farhad Salek, Shahaboddin Resalati, Meisam Babaie, Paul Henshall, Denise Morrey, and Lei Yao. A review of the technical challenges and solutions in maximising the potential use of second life batteries from electric vehicles. *Batteries*, 10(3):79, 2024. Number: 3 Publisher: Multidisciplinary Digital Publishing Institute.

[93] Xiaofan Cui, Muhammad Aadil Khan, Gabriele Pozzato, Surinder Singh, Ratnesh Sharma, and Simona Onori. Taking second-life batteries from exhausted to empowered using experiments, data analysis, and health estimation, 2024.

[94] Zubayer Islam, Mohamed Abdel-Aty, Qing Cai, and Jinghui Yuan. Crash data augmentation using variational autoencoder. *Accident Analysis & Prevention*, 151:105950, 2021.

[95] David Kornish, Soundararajan Ezekiel, and Maria Cornacchia. DCNN augmentation via synthetic data from variational autoencoders and generative adversarial networks. In *2018 IEEE Applied Imagery Pattern Recognition Workshop (AIPR)*, pages 1–6, 2018. ISSN: 2332-5615.

[96] Zhiqiang Wan, Yazhou Zhang, and Haibo He. Variational autoencoder based synthetic data generation for imbalanced learning. In *2017 IEEE Symposium Series on Computational Intelligence (SSCI)*, pages 1–7, 2017-11.

[97] Chang Liu, Ruslan Antypenko, Iryna Sushko, and Oksana Zakharchenko. Intrusion detection system after data augmentation schemes based on the VAE and CVAE. *IEEE Transactions on Reliability*, 71(2):1000–1010, 2022. Conference Name: IEEE Transactions on Reliability.

[98] Lucas Pinheiro Cinelli, Matheus Arajo Marins, Eduardo Antnio Barros da Silva, and Srgio Lima Netto. Variational autoencoder. In Lucas Pinheiro Cinelli,

Matheus Arajo Marins, Eduardo Antnio Barros da Silva, and Srgio Lima Netto, editors, *Variational Methods for Machine Learning with Applications to Deep Networks*, pages 111–149. Springer International Publishing, 2021.

[99] Keras Team. Keras documentation: Variational AutoEncoder. https://keras.io/examples/generative/vae/, 2024.

[100] Mohammed Wadi. Fault detection in power grids based on improved supervised machine learning binary classification. *Journal of Electrical Engineering*, 72(5):315–322, 2021.

[101] Aized Amin Soofi and Arshad Awan. Classification techniques in machine learning: Applications and issues. *Journal of Basic & Applied Sciences*, 13:459–465, 2017.

[102] Yuyi Tan, Tianpei Liu, Xingbin Ye, Yanhua Chen, Qingcheng Yang, and Weiwen Peng. Early prediction method for remaining useful life of retired batteries in second-life applications. In *2022 4th International Conference on System Reliability and Safety Engineering (SRSE)*, pages 522–530, 2022.

[103] Afef Saidi, Slim Ben Othman, Meriam Dhouibi, and Slim Ben Saoud. FPGA-based implementation of classification techniques: A survey. *Integration*, 81:280–299, 2021.

[104] Sameena Pathan, K. Gopalakrishna Prabhu, and P. C. Siddalingaswamy. Techniques and algorithms for computer aided diagnosis of pigmented skin lesionsa review. *Biomedical Signal Processing and Control*, 39:237–262, 2018.

[105] Ivn Sanz-Gorrachategui, Pablo Pastor-Flores, Milutin Pajovic, Ye Wang, Philip V. Orlik, Carlos Bernal-Ruiz, Antonio Bono-Nuez, and Jess Sergio Artal-Sevil. Remaining useful life estimation for LFP cells in second-life applications. *IEEE Transactions on Instrumentation and Measurement*, 70:1–10, 2021. Conference Name: IEEE Transactions on Instrumentation and Measurement.

[106] UL 1974: Creating a safe second life for electric vehicle batteries. https://www.ul.com/resources/ul-1974-creating-safe-second-life-electric-vehicle-batteries.

Appendix A

A.1 ECM Fitting and Model Visualization

Circuit Element	Value	Unit
L_1	5.00×10^{-8}	H
R_{bulk}	5.00×10^{-3}	Ω
R_{sei}	5.00×10^{-4}	Ω
C_1	$3.00 \times 10^{+0}$	F
R_{ct}	5.00×10^{-3}	Ω
R_w	1.00×10^{-2}	Ω
$Z_{w,\tau}$	$5.00 \times 10^{+1}$	s
C_2	1.00×10^{-2}	F

Table A.1: Initial guesses for the equivalent circuit elements.

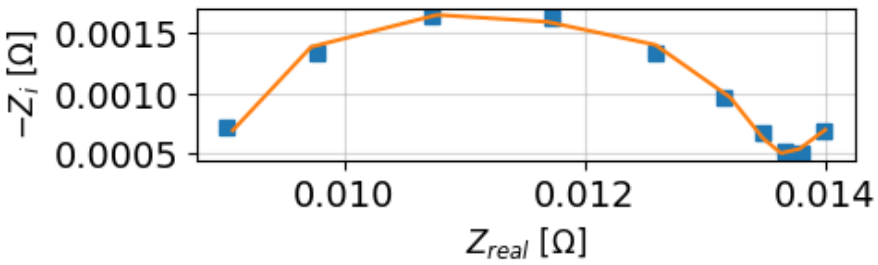

(a) ECM Fitting at the beginning of life

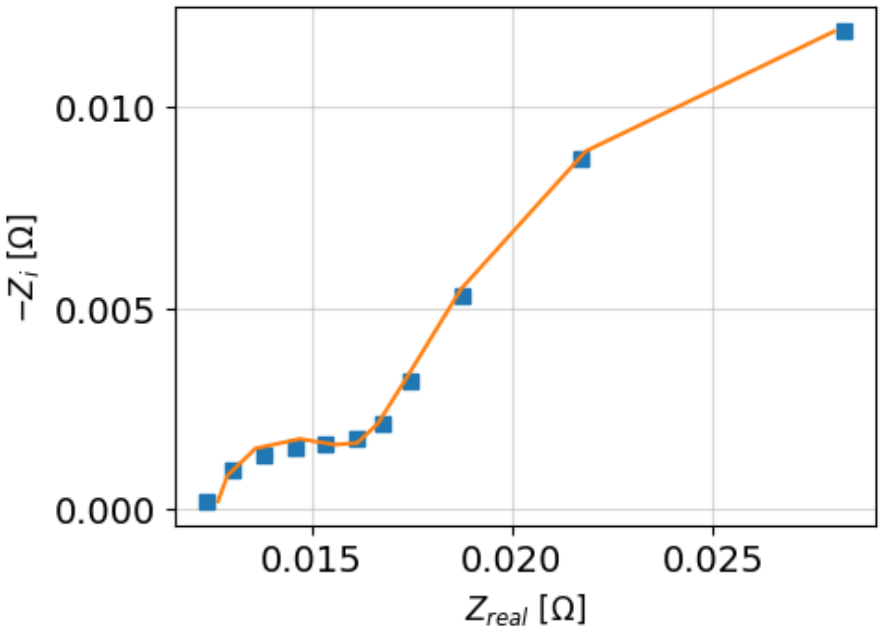

(b) ECM fitting at the end of life

Figure A.1: Nyquist plot fitting using equivalent circuit model at different stages: (a) Initial condition, and (b) Final condition.

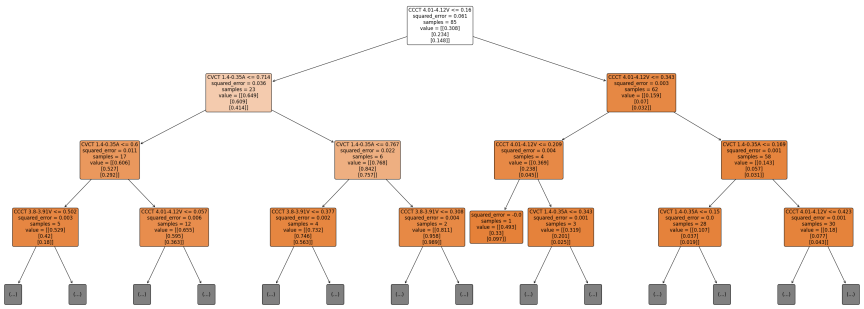

Figure A.2: A decision tree from the random forest training process.

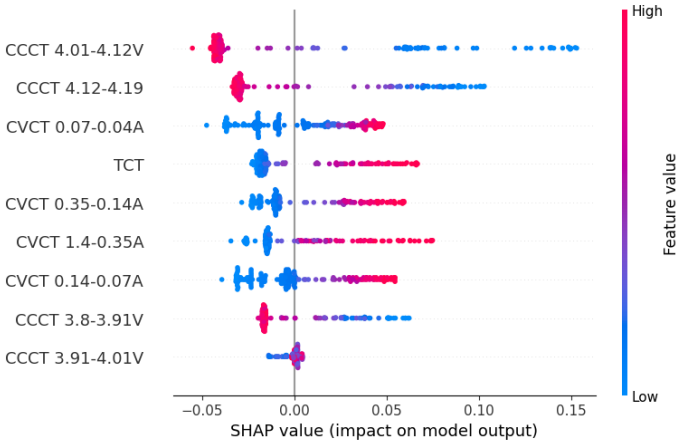

(a) Conductivity loss

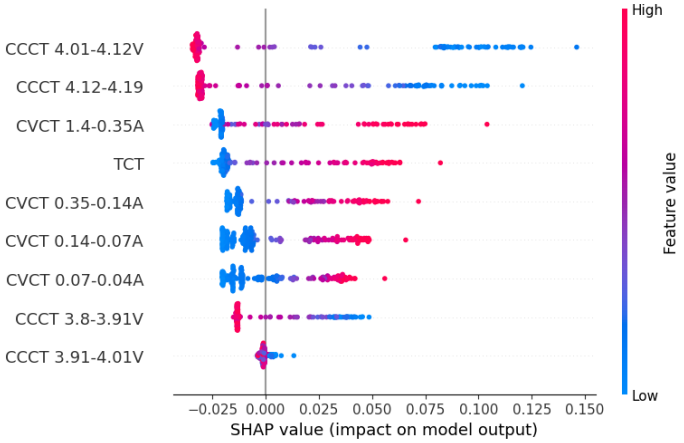

(b) Loss of lithium inventory

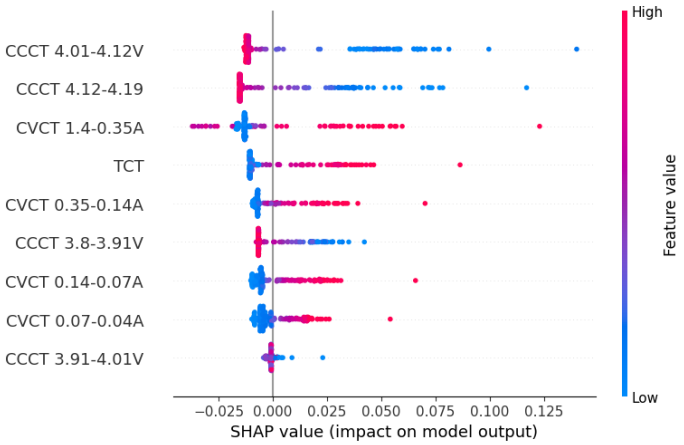

(c) Loss of active material

Figure A.3: Shap bee plot for each degradation mode from the training of the multi-output regression random forest model.

A.2 ECM Fitting and Additional Results

A.2.1 ECM Fitting

Circuit Element	Value	Unit
L_1	5.00×10^{-6}	H
R_{bulk}	5.31×10^{-1}	Ω
R_{sei}	4.77×10^{-1}	Ω
CPE_1	4.47×10^{-2}	$\Omega^{-1}\,s^a$
$CPE_{1,\alpha}$	5.77×10^{-1}	-
R_{ct}	9.69×10^{-1}	Ω
CPE_2	6.21×10^{-2}	$\Omega^{-1}\,s^a$
$CPE_{2,\alpha}$	$1.00 \times 10^{+0}$	-
R_w	$2.65 \times 10^{+1}$	Ω
$Z_{w,\tau}$	$1.02 \times 10^{+4}$	s

Table A.2: Initial guesses for the equivalent circuit elements.

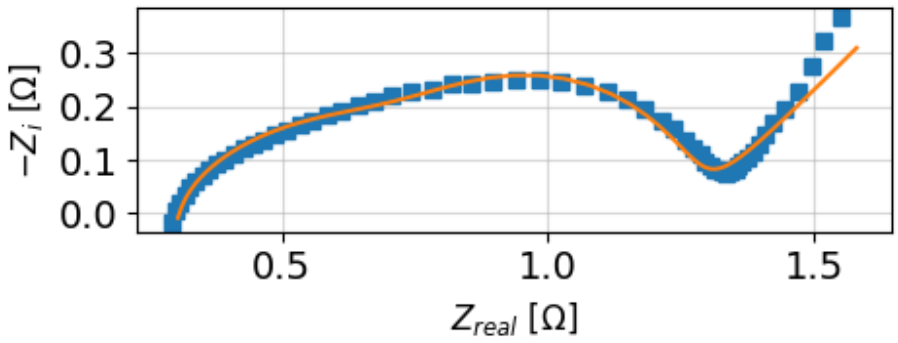

(a) ECM fitting at beginning of life

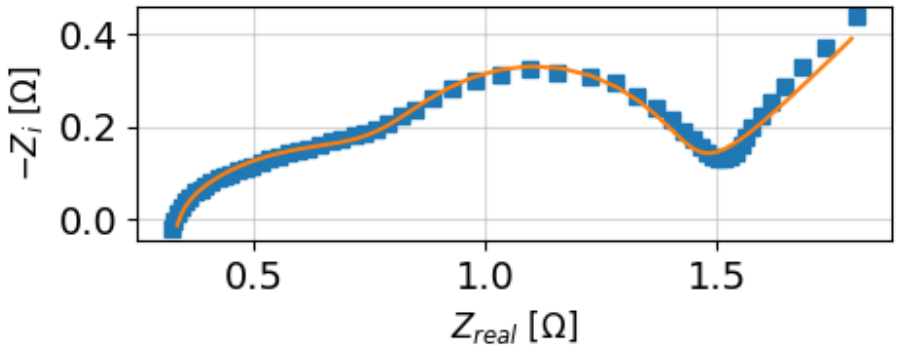

(b) ECM fitting at the end of second life

Figure A.4: Nyquist plot fitting using equivalent circuit model at different stages: (a) Initial condition, and (b) Final condition.

A.2.2 VAE Loss Function Definition

The Kullback-Leibler loss is defined by:

$$\text{KL loss} = -0.5 \cdot \sum \left(1 + z_{\text{log\_var}} - z_{\text{mean}}^2 - e^{z_{\text{log\_var}}}\right)$$

- z_{mean}: Mean of the latent variable z, predicted by the encoder.
- $z_{\text{log\_var}}$: Logarithm of the variance of z, predicted by the encoder.

The weighted reconstruction loss is given by:

$$\text{reconstruction\_loss} = \sum_{i=1}^{n} w_i \cdot \mathbb{E}\left[(x_i - \hat{x}_i)^2\right]$$

- w_i are the weights for each feature ($w_i = 1$ for ECM parameters, $w_7 = 3$ for the RUL).
- x_i is the i-th feature of the input.
- $\hat{x}_i$ is the i-th feature of the decoded feature.
- $\mathbb{E}[\cdot]$ denotes the mean along the batch dimension.

Explicitly, this becomes:

$$\text{reconstruction\_loss} = \sum_{i=1}^{6} \mathbb{E}\left[(x_i - \hat{x}_i)^2\right] + 3 \cdot \mathbb{E}\left[(x_7 - \hat{x}_7)^2\right]$$

Where the first six features have weights of 1, and the seventh feature has an increased weight of 3.

A.2.3 Training

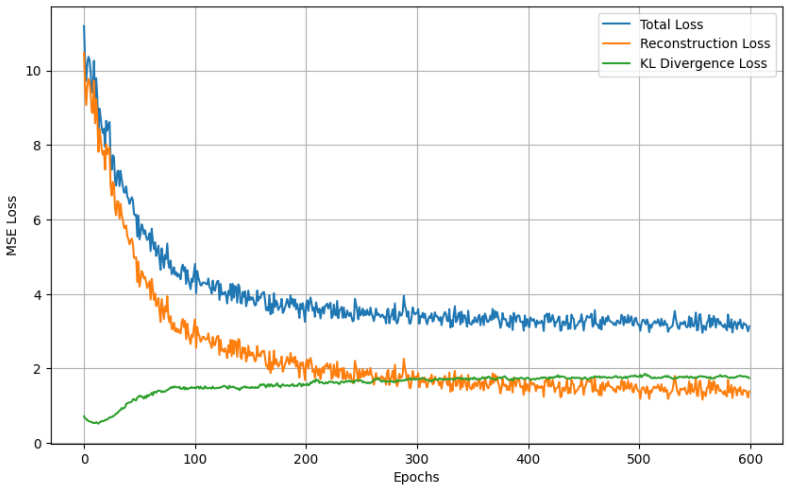

Figure A.5: Reconstruction, KL, and total loss progression over VAE training.

A.2.4 Synthetic Data Results

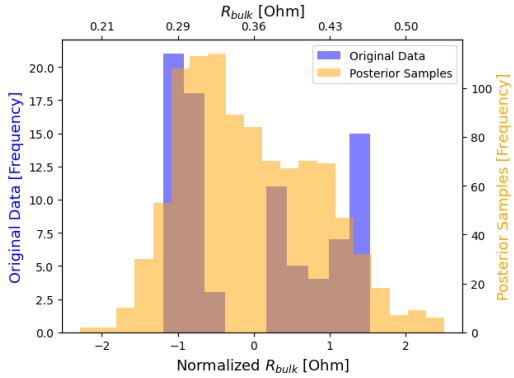

(a) R_{bulk}

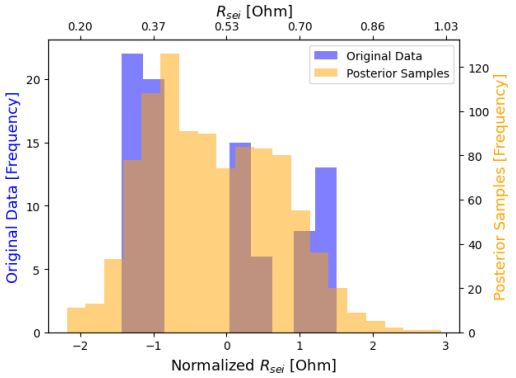

(b) R_{SEI}

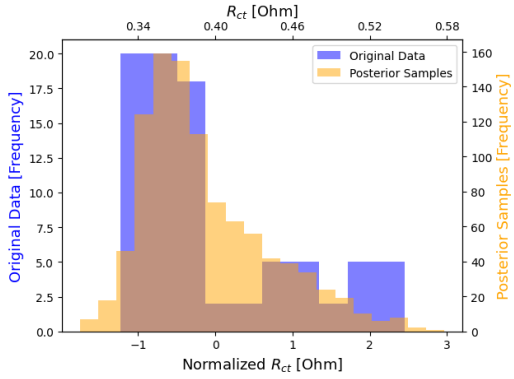

(c) R_{ct}

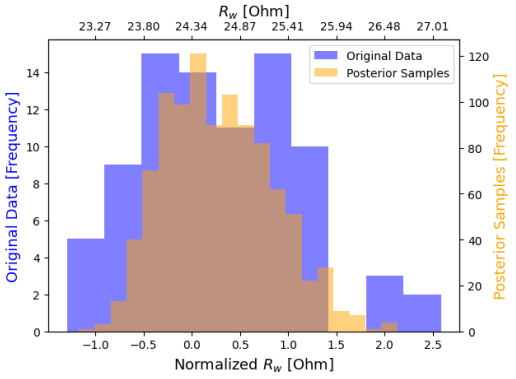

(d) R_w

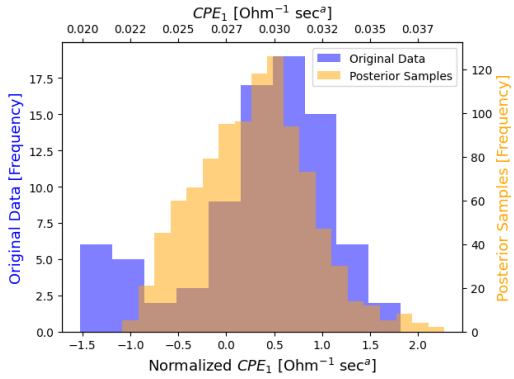

(e) CPE_1

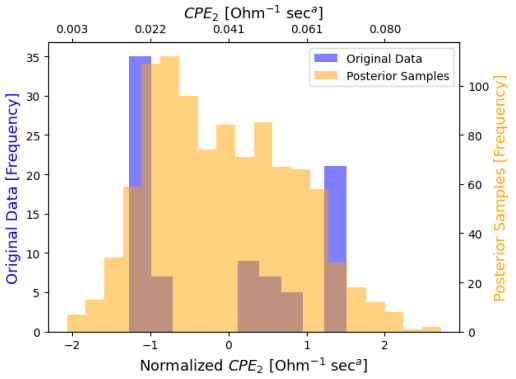

(f) CPE_2

Figure A.6: Histograms of model parameters related to impedance analysis (R_{bulk}, R_{SEI}, R_{ct}, R_w, CPE_1, CPE_2).

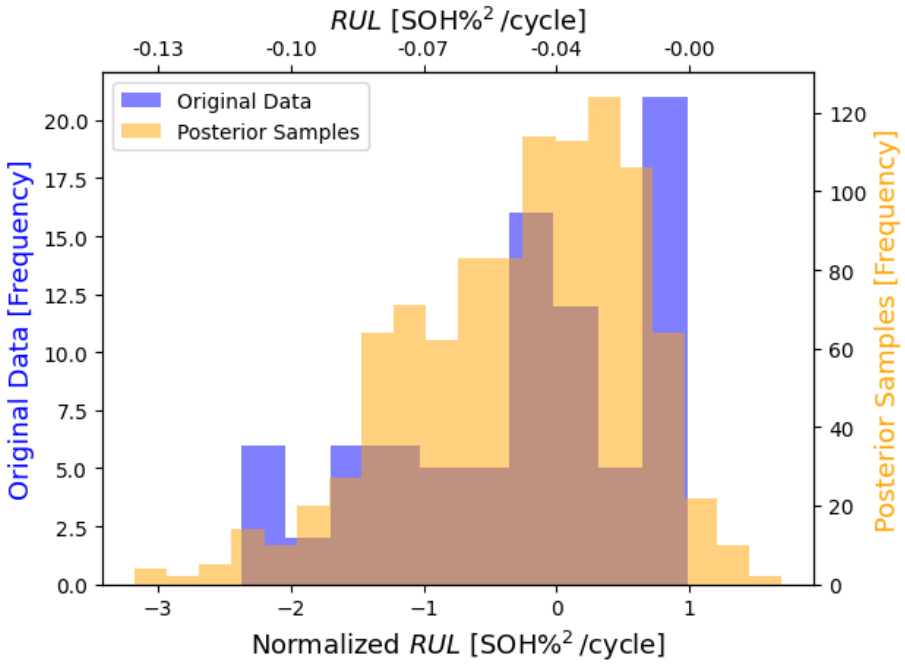

Figure A.7: Histogram of Remaining Useful Life (RUL).

A.2.5 ECM inputs

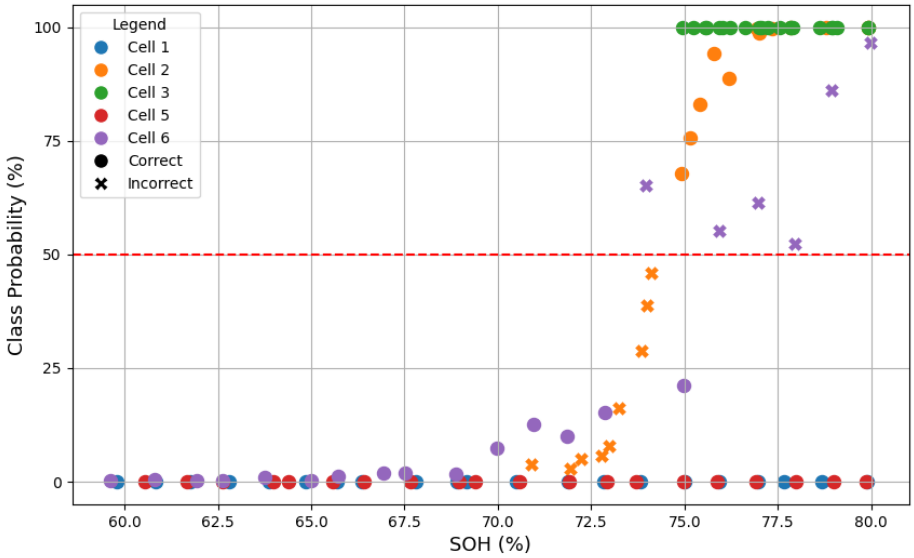

Figure A.8: Plot for 5% loss per 100 cycles

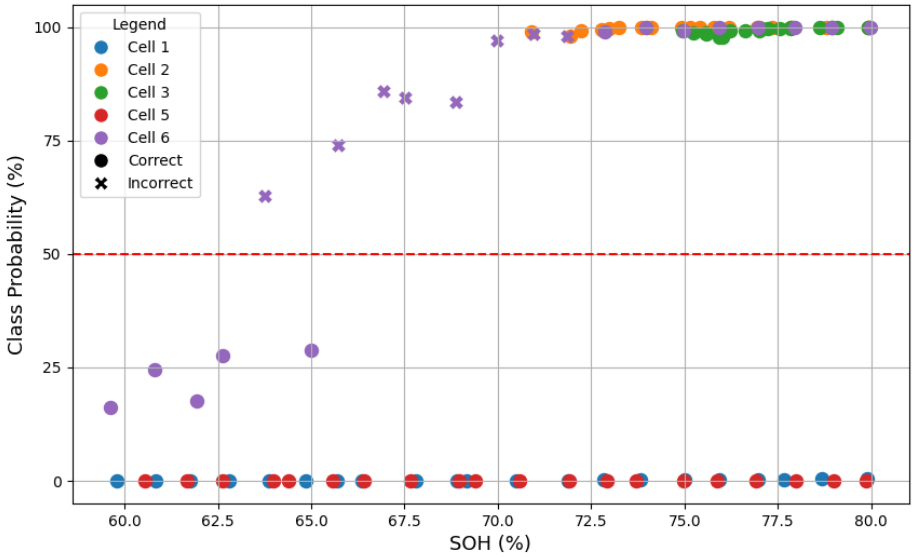

Figure A.9: Plot for 10% loss per 100 cycles

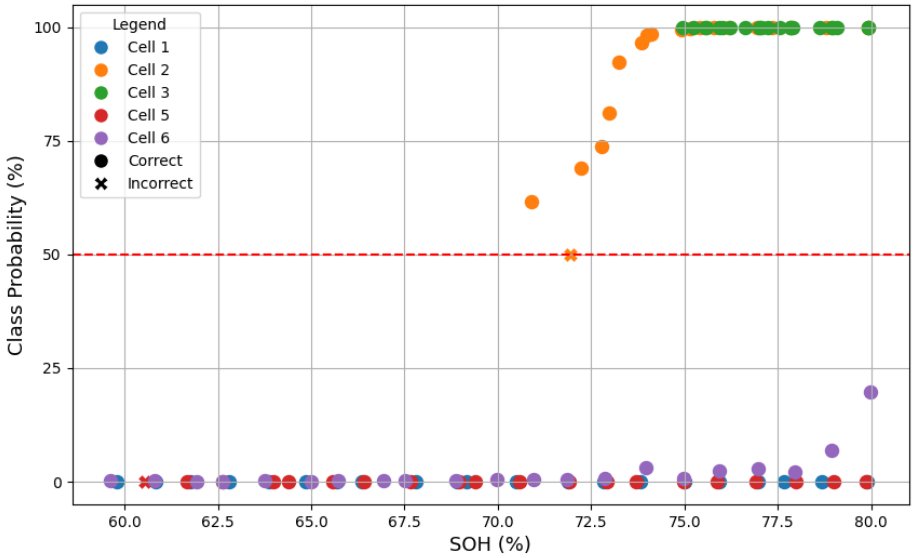

Figure A.10: Plot for 75/25 split

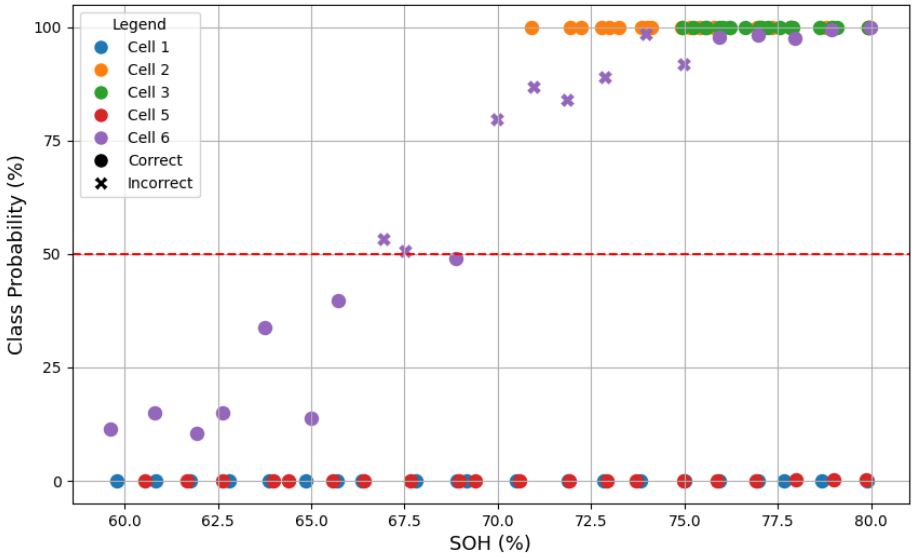

Figure A.11: Plot for 50/50 split

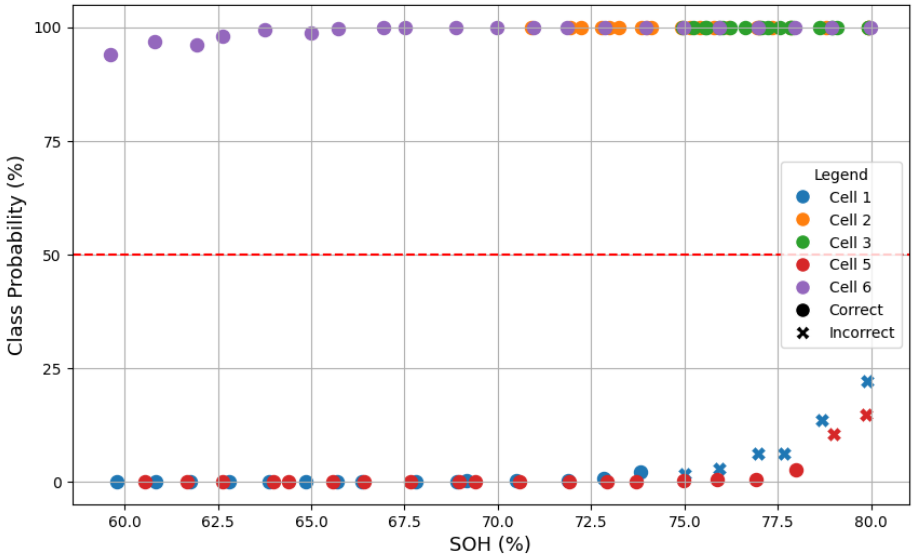

Figure A.12: Plot for 25/75 split

A.2.6 SOH input

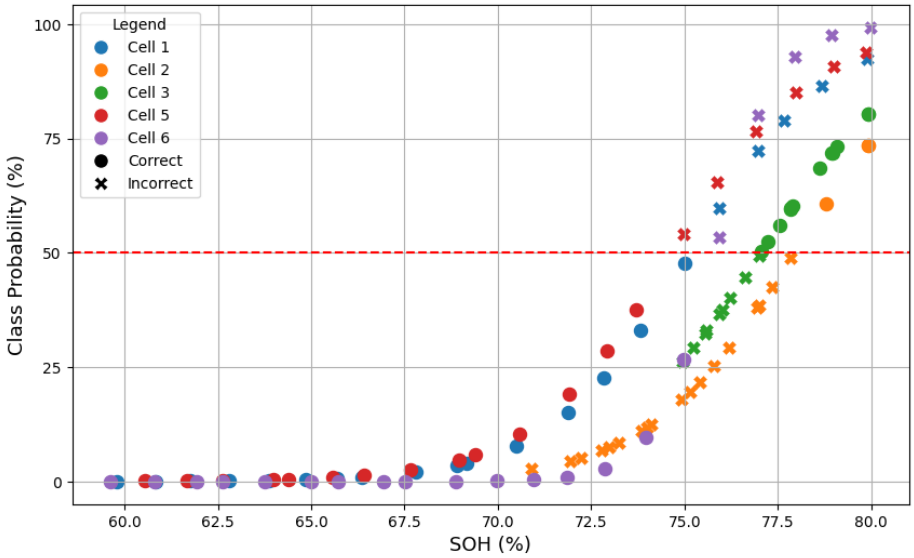

Figure A.13: SOH plot for 5% loss per 100 cycles

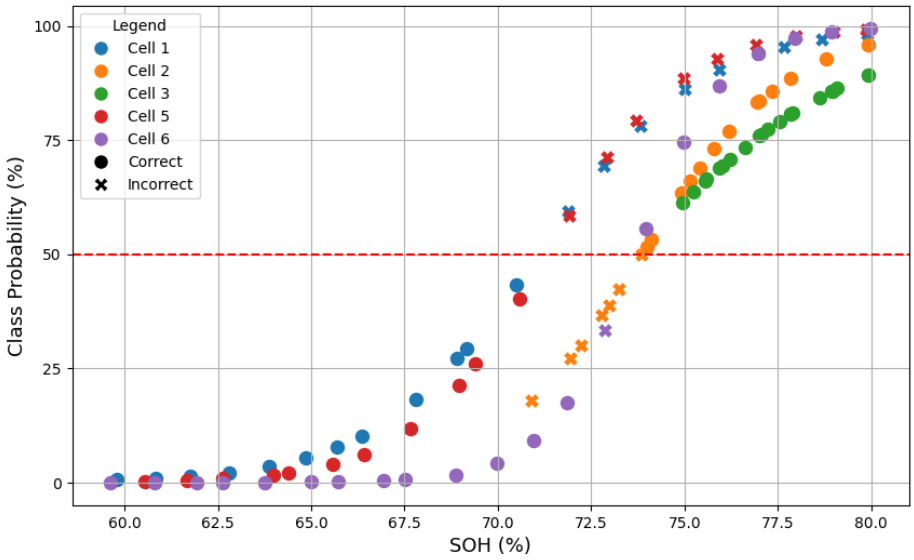

Figure A.14: SOH plot for 10% loss per 100 cycles

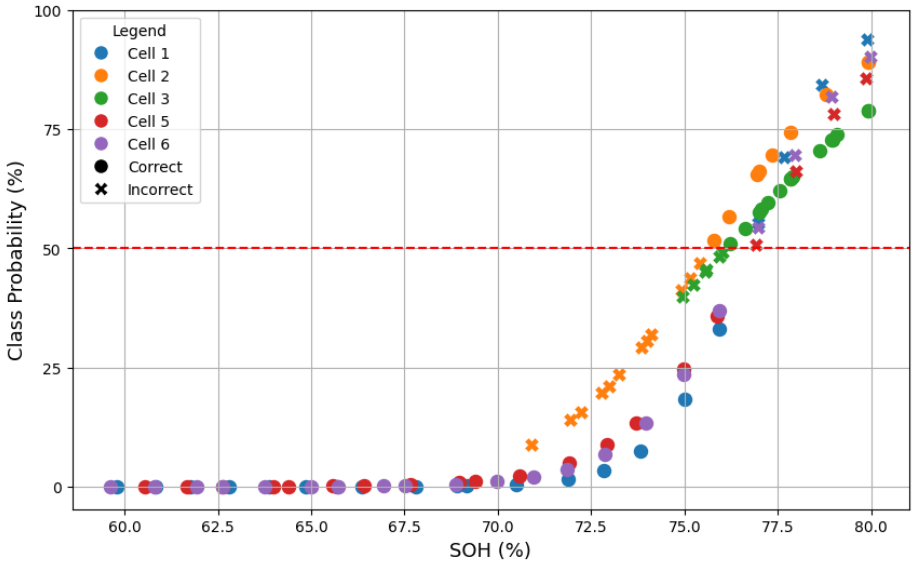

Figure A.15: SOH plot for 75/25 split

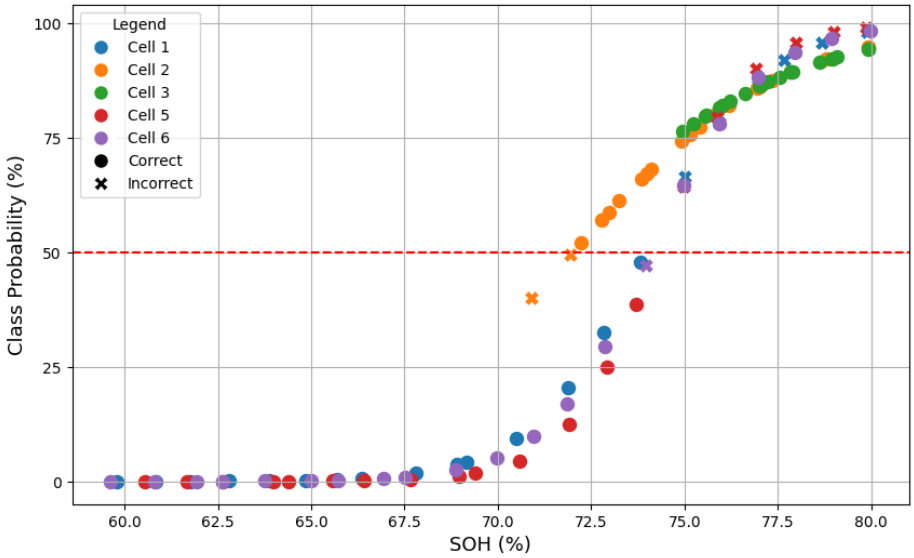

Figure A.16: SOH plot for 50/50 split

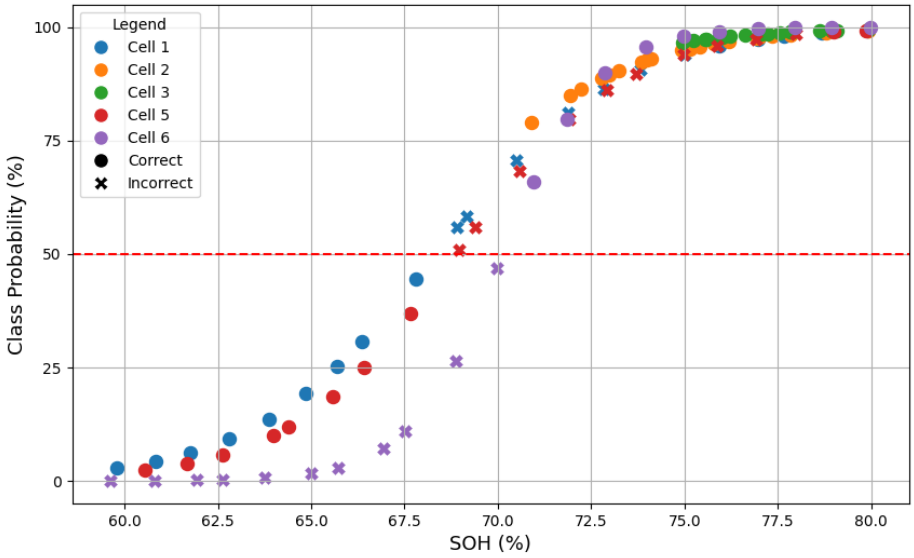

Figure A.17: SOH plot for 25/75 split